journal of the international meteor organization

# WGN

51:5
october 2023



ISSN 1016-3115

WGN Vol. 51, No. 5, October 2023, pp. 109 – 142

## Administrative



## Conferences



## Ongoing meteor work



## Preliminary results



## Front cover photo

Bright fireball captured on 2023 April 6 at $06^{h}48^{m}$ UT from Crestone, Colorado, USA. While it looks like daytime it is actually the full Moon illuminating the landscape. Image courtesy: Mike Lewinski.

## Writing for WGN

This Journal welcomes papers submitted for publication. All papers are reviewed for scientific content, and edited for English and style. Instructions for authors can be found in WGN **45:1**, 1–5, and at `http://www.imo.net/docs/writingforwgn.pdf` .

## Copyright



## Legal address

International Meteor Organization, Jozef Mattheessensstraat 60, 2540 Hove, Belgium.

# Guest Editorial

*Marc Gyssens*

Of course, you have already read in the August issue the enthusiastic report on the once again very successful IMC 2023 in Redu, Belgium, by (on-site) participants Greet Lembregts and Marthe D'Hooghe, and, therefore, it is not my intention to repeat what has already been written there. Rather, I want to continue on my guest editorial in the October 2022 issue of WGN and share with you what the IMC 2023 meant to me as Founding Member and long-time Council Member of our Organization.

I mentioned in my previous guest editorial that, at the IMC 2022 in Poroszló, Hungary, the first one ever in hybrid format, we had only 52 on-site participants, but 104 online participants. It seemed that, with the lockdowns during the Covid-19 pandemic still fresh in mind, many people did not yet trust if after the cancellation of the 2020 and 2021 events. This year, we had 86 on-site participants and only 44 online participants. The smaller number of online participants may be explained by the fact that we asked online participants a small fee of 20 EUR as contribution to the costs involved in setting up a hybrid event. The main thing to take away from these numbers in my opinion, however, is that the distribution of the participants shifted from 1/3 on site and 2/3 online to 2/3 on site and 1/3 online! This, to me, is a very encouraging evolution. Meteor workers find their way back to the IMC location, and that is very important, because, besides the scientific content of the program, the personal interaction among meteor workers is the greatest added value of this conference!

One of the characteristics of the IMC 2022 was the presence of many young and enthusiastic first-time attendants. It was heart-warming to see that many of these became IMO member and were present again at the IMC 2023. Some of them even assumed responsabilities within the IMO, despite becoming a member so recently! And this year, too, we saw again several young first-time attendants which were equally enthusiastic and registered as an IMO member at the conference. To me, this only confirmed my feeling that a much-needed rejuvenation of our Organization has been set in!

In my previous guest editorial, I observed that "the meteor scene evolved from a group of amateurs and a group of professionals which were on speaking terms with each other to a very closely knit community in which the boundary between amateurs and professionals had faded completely". This was illustrated at the IMC 2023 in a very compelling way by the first session on Thursday evening, which was entirely devoted to the discovery, impact, and recovery of fragments of the small asteroid 2023 CX1 during the days following February 12, 2023. The entire chain of events was covered, from the discovery by Krisztián Sárneczky, co-organizer of the IMC 2022 in Hungary over the observations of the fireball (of which many reports were submitted to the IMO) to the recovery of fragments by the people of FRIPON/Vigie Ciel with the guidance of Peter Jenniskens. The astounding efficiency of this endeavor and the fact that many people involved in it are either IMO member or closely linked to our Organization were the most convincing testimony to my statement of last year. Without any doubt, the IMO and its annual conference, the IMC, have played a katalyzing role in this development! For many participants, that session was one of the highlights of the conference.

As already mentioned, the IMC 2022 was the first one to be organized as a hybrid event. That year, and perhaps to be expected, we experienced some minor, but nevertheless annoying, difficulties. However, we learnt from it and finetuned everything, and in conjunction with the excellent infrastructure of the Euro Space Center, the venue of the IMC 2023, this resulted in a smooth conference for both on-site and online participants.

A last point I want to mention regards the General Assembly Meeting of the IMO, which is traditionally held in conjunction with the IMC, usually on the Friday evening, as was also the case in 2023. Because we need to change our Constitution to conform to a change in the Belgian Law (the IMO is an international non-profit organization under Belgian Law), two thirds of our Voting Members[1] had to be present or represented. Although I was maybe the last person to believe that we could actually achieve this, it turned out that in the end 196 of the 249 Voting Members were present (physically or online) or represented (via proxy), 30 more than strictly needed! In this sense, a lot more people than the 130 on-site and online participants were involved in an aspect of the IMC 2023! At the General Assembly Meeting, it was decided to bring the proposal to change the Constitution to the ballot. Of course, this ballot is secret and, to this end, the system is set up in such a way that nobody can see intermediate results until the ballot closes on December 1, but what I can see and say is that as of now 189 Voting Members have already cast their vote, so once again we have reached the two-thirds quorum required for a valid result. My reason for sharing this with you is to illustrate once again the level of commitment within our Organization. We may truly say that the IMO is a meteor *community* which, when it works towards a common goal, can achieve great results, as the events on and after February 12 prove.

So, the good feeling that remained with me after the IMC 2022 was only confirmed by the IMC 2023, and I am quite confident that this will be no different for the IMC 2024!

[1] New members enter the IMO as Associate Member. Within one or two years, Associate Members usually see their status changed to Voting Member.

Finally, I must thank once again the editor-in-chief, my good friend Javor, to allow me to write this guest editorial and for composing once again an exciting issue of WGN – and as a former editor-in-chief myself, I know this is not a light task. So, I will end with the words with which I ended so many of my editorials in the past:

Happy reading!

IMO bibcode WGN-515-gyssens-editorial NASA-ADS bibcode 2023JIMO...51..109G

# From the Treasurer — IMO Membership/WGN Subscription Renewal for 2024

*Marc Gyssens*

## Renewal rates

All members/subscribers whose membership/subscription expires at the end of 2023 are kindly invited to renew for 2024. If you are not sure when your membership/subscription expires, log in to your IMO account. Under your profile picture (or its placeholder in case you have no profile picture) you will see a green banner telling you when your membership will expire. (If you do not see you profile page upon logging in, go to the pull-down menu labeled with your name in the right upper corner – "your profile" is the first item!)

Even if you happen to make a mistake, however, and you "renew" despite already having paid for 2024, no harm is done: your payment will be used for the first year after the current expiration date of your membership/subscription!

The fees are as tabulated below. Notice that the membership/subscription fees have remained unchanged!

| IMO Membership/WGN Subscription 2024 | | | | |
|---|---|---|---|---|
| Electronic + paper with surface mail delivery: | | €26 | | US$ 30 |
| Electronic + paper with airmail delivery (outside Europe only): | | €49 | | US$ 56 |
| Electronic only: | | €21 | | US$ 24 |
| Supporting membership: | add | €26 | add | US$ 30 |

It is also possible to renew for two or more years in a row.

When you renew, give a few minutes of thought to becoming a **supporting member** by paying at least 26 EUR/30 USD extra. Smaller gifts are of course also appreciated. As you may know, there is an IMO Support Fund. With this Support Fund, we offer support to meteor-related projects. Our ability to provide this service to the meteor community depends primarily on the gifts we receive from supporting members!

Another way to help meteor workers with limited funds is to offer them a gift subscription.

We already thank all our members that will renew for their continued trust in our Organization!

## Payment instructions

You first must log in into your account at the IMO website if you want to renew. For this purpose, click the log-in button in the upper right-hand corner. In case you forgot your password, you can use the "forgot password" link to reset it. If the green banner below your profile picture (or its placeholder) tells you that your membership/subscription is about to expire – see above, click on it, and the rest will be self-explanatory.[1]

The outcome of this process is that you will see the total amount due and your payment options. If you choose to pay using PayPal (or using a credit card via PayPal), you can complete the payment on our website.

If you experience any difficulties, do not hesitate to contact me at `treasurer@imo.net`.

One final request: every year, a lot of members renew late. As a consequence, back issues that already appeared have to be sent out to these members. Please support our volunteers in their bimonthly effort to process WGN by renewing promptly! Thank you for your understanding and cooperation!

IMO bibcode WGN-515-gyssens-renewal NASA-ADS bibcode 2023JIMO...51..110G

[1] Alternatively, you can also click on "Extend your membership" in the pull-down menu labeled with your name in the upper right-hand corner, with the same result.

# Conferences

## Save the Date: Forty-Third International Meteor Conference, Kutná Hora, Czech Republic, September 19–22, 2024

*communicated by Marc Gyssens*

During the General Assembly Meeting of the IMC 2023, it was announced that the 43th International Meteor Conference (IMC 2024) will take place in Kutná Hora, in the Czech Republic, from September 19–22, 2024.

The Local Organizing Committee consists of members of the Meteor Physics Group, Department of Interplanetary Matter, Astronomical Institute of the CAS, in Ondřejov, and is chaired by Pavel Koten. As most of you know, Ondřejov Observatory is the center of the European Fireball Network, the longest operating project for monitoring of bright meteors in the world. Its origins date back to the middle of the 20th century, when Zdeněk Ceplecha, a famous meteor scientist, laid the foundation of this Network.

With the important role that Ondřejov Observatory has played in meteor science in mind, it is quite remarkable that there has not yet been an IMC in the Czech Republic. This anomaly will finally be removed with its 43th edition, in 2024!

The location of the IMC 2024 will be the small city of Kutná Hora (ca. 21 000 inhabitants). It has a rich history going back to the middle ages, mainly due to silver mining activity, and is also an architectural gem. Just like Prague, it figures on the UNESCO World Heritage List. The excursion at the IMC 2024 will consist of a guided tour of the city. Kutná Hora is also conveniently located, at 50 km from Prague, with which it is well connected by road, train, and bus.

The conference will take place from Thursday evening, September 19 until Sunday noon, September 22, 2024. The dates have been chosen in such a way that interested participants may combine it with the Europlanet Science Congress in Berlin from September 8 to 14, 2024. Of course, the IMC 2024 can also be combined with a visit to Prague before or after the Conference. Finally, a visit to Ondřejov Observatory (ca. 30 km south of Prague) is also possible after the Conference.

More detailed information about the IMC 2024 will be available soon, via WGN and the IMO website!

*Figure 1* – The city of Kutná Hora, listed as a UNESCO World Heritage site, is the location of the IMC 2024.

# Ongoing meteor work

## The Meteor Orbit Association Tool v1.0 (MOAT): An Interactive Graphical User Interface MATLAB Program

*David Holman* [1]

The Meteor Orbit Association Tool v1.0 is presented. This graphical user interface MATLAB program uses 6 large interactive plots for evaluation of the orbital similarity of meteor radiants, verification of that similarity in orbital element space, and determining the resulting radiant cluster's significance against the background. The compiled app uses publically available video meteor orbit data, and new data files can be loaded to the app. Meteor Data Center IAU#'s 1–1211 are included in the shower catalog, and Search mode allows new radiant clusters to be examined. Ten D criteria functions and many display options are available. The MOAT app runs on MATLAB Runtime, and both are free downloads.

Received 2023 August 17

### 1 Introduction

The Meteor Orbit Association Tool v1.0 (Moat) was created to provide amateur meteor researchers with a user friendly app to evaluate the orbital similarity of meteor radiants derived from video triangulation, and to verify that similarity for working showers and newly discovered radiant clusters prior to dynamical analyses to identify a common parent body. Written with Matlab R2022b on Windows 10, the Moat app runs on Matlab Runtime. The Moat app and data folder is free download from Google Drive, and Matlab Runtime is a free download from MathWorks.

[1]5990 SE King Rd. #41, Milwaukie, OR, 97222 USA.
Email: daveh@lmi.net

IMO bibcode WGN-515-holman-moat
NASA-ADS bibcode 2023JIMO...51..112H

Moat displays meteor radiants using 3 pairs of plot types: equatorial coordinates, ecliptic coordinates, and orbital element space. The graphical user interface (GUI) is shown in Figure 1. Each plot type has overlay and removal plots where assigned D criteria radiants are overlaid with a colored marker and removed from the background radiants, respectively (Figure 2). The GUI was designed on a monitor with 1600 × 900 pixel resolution. Smaller monitors may compromise the GUI.

All plots are interactive so any radiant marker can be clicked on to display the orbital elements. The selected radiant can be used as the comparison orbit for a D criteria application. This process can be used to identify new radiant clusters, or repeated as an iterative application of a D function on larger, denser radiant clusters.

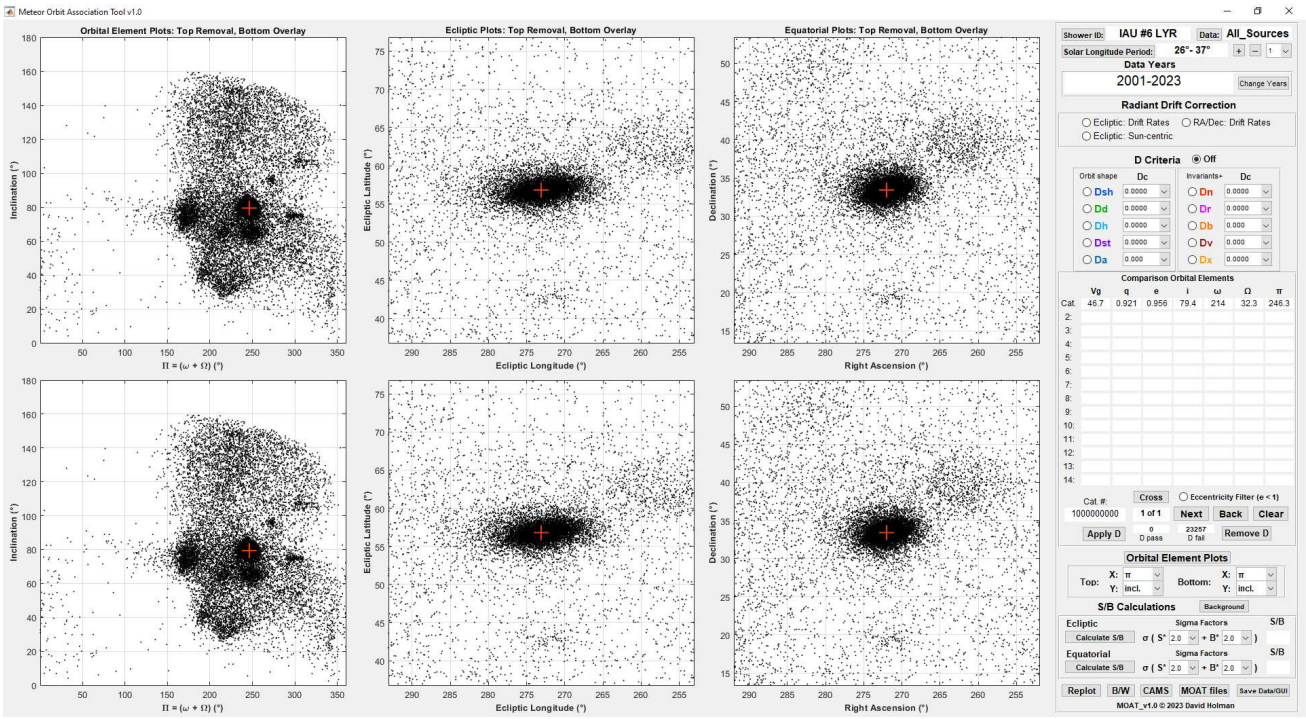


*Figure 1* – The layout of the Moat GUI upon opening showing the Lyrids IAU #6. The radiants displayed are a combination of CAMS, SonotaCo, EDMOND/Nfc/BRAMON, CMN, and GMN data. Each D criteria function plots in a different color. The orbital element plots are in **Full View** display.

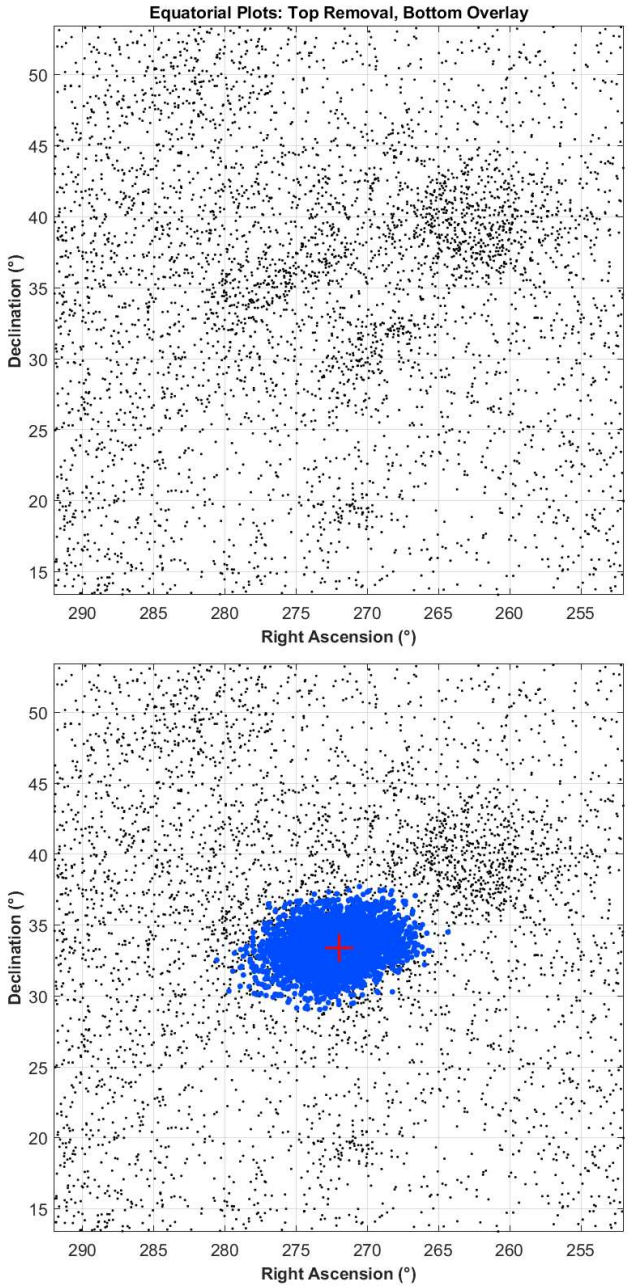


*Figure 2* – The right most plots from Figure 1 with most of the Lyrids removed from the background using 3 iterations of **Dsh** (orbital elements shown in the 3 dark grey (green in electronic *WGN*) lines of Figure 3). The **Eccentricity Filter** is activated.

Text files of the assigned meteor radiants orbital elements are made automatically that record every D criteria change, solar longitude or data year(s) changes, and D criteria iterations being added, removed, or changed. An image file of the GUI and a full list of assigned and unassigned radiants can be saved at any time.

The app folder contains publicly available meteor orbit data from Cameras for Allsky Meteor Surveillance (CAMS), SonotaCo Network, European viDeo Meteor Observation Network Database (EDMOND)/Central European Meteor Network Narrow Field Camera (Nfc)/ BRAzillian MeteOr Network (BRAMON), Croatian Meteor Network (CMN), and the Global Meteor Network (GMN) (Jenniskens et al., 2018; SonotaCo, 2009; SonotaCo, 2016; SonotaCo, 2017; SonotaCo et al., 2021; Kornoš et al., 2014a; Kornoš et al., 2014b; Korlević et al., 2013; Vida et al., 2020; Vida et al., 2021, respectively) and when fully loaded Moat has access to over 2.1 million radiants. A data set combining all sources is also loaded, and is the data shown in the Figures.

The Moat shower catalog lists 979 showers IAU #'s 1–1211 from the Meteor Data Center (MDC) and is easily edited. The shower catalog and meteor orbit data sets can also be replaced with new data, and the app guides the process. In Search mode Moat can be aimed at a new shower using location coordinates and solar longitude so suspected radiant clusters can be examined.

## 2 MOAT Features

Figure 3 is a close-up of the Moat control panel for the plots in Figure 2, and the features will be listed from the top down. The button and text panel names are in **bold**.

**Shower ID** button and panel: The panel shows the shower ID (IAU # and code) and the button changes the shower.

**Data** button and panel: The panel shows the data source being displayed and the button changes the data source.

**Solar Longitude Period** button and panel: The panel shows the solar longitude range and the button resets the solar longitude range to the cataloged or input values at the start.

**+/−:** Increase or decrease the solar longitude period by the increment selected (1–10) from the drop-down menu.

**Data Years:** This panel shows the range or selection of years the displayed data spans.

**Change Years:** Select the years of data to display.

**Drift Rates/Sun-centric:** Apply drift rate corrections, or shift the Ecliptic plots to sun-centric.

**Dsh, Dd, Dh, Dst, Da, Dn, Dr, Db, Dv,** and **Dx:** Ten D criteria functions, with the thresholds, $D_c$, selected from the drop-down menus (Southworth and Hawkins, 1963; Drummond, 1981; Jopek and Froeschlé, 1997; Steel et al., 1991; Asher et al., 1993; Valsecchi et al., 1999; Jenniskens, 2008; Jopek et al., 2007; Rudawska et al., 2015, respectively).

**Iteration Viewer:** Activated by clicking any of the **Comparison Orbit Elements** panel's labels **(Cat., 2:, 3:**, etc.) after the second iteration has been made. View any selection of iterations.

**Cross:** Toggles the center cross in and out of the plots.

**Eccentricity Filter:** Removes all radiants with eccentricity $e \geq 1$.

**Next, Back, Clear:** Select among a group of interactively captured radiants, or clear the captured radiants.

**Apply D, Remove D:** Apply the active D function to the current iteration, or remove it.

**D Pass, D Fail:** These panels list the number of assigned and unassigned radiants, respectively.

**Orbital Element Plots:** This button selects either **Full View** or **Detail** for the orbital element plots.

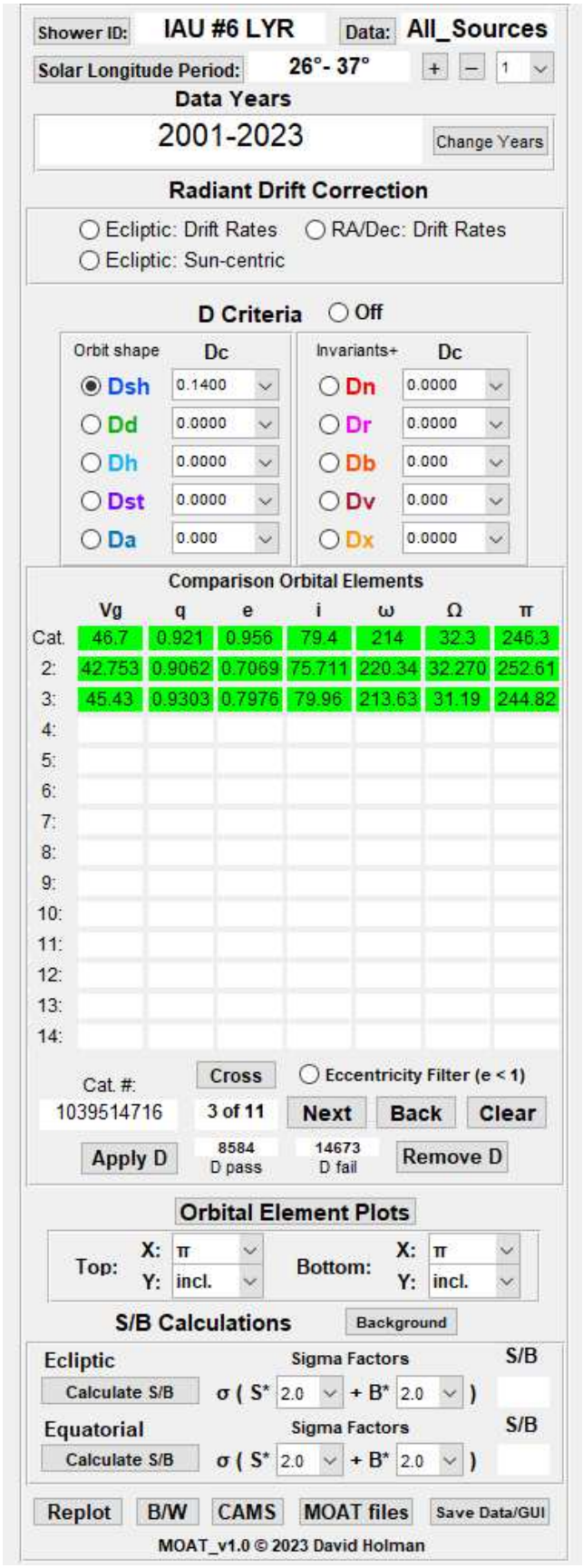


*Figure 3* – The Moat control panel, showing the work done for Figure 2.

**Top: X Y** and **Bottom: X Y:** Set the plot axes to an element: perihelion ($q$), $e$, inclination ($i$), periastron ($\omega$), ascending node ($\Omega$), aphelion, longitude of perihelion ($\Pi$), geocentric velocity ($V_g$), absolute visual magnitude, the Tisserand parameter with respect to Jupiter, semi-major axis ($a$), $1/a$, the D criteria value, Sun-centered ecliptic longitude, ecliptic latitude, Right Ascension (R.A.), Declination (Decl.), and Solar longitude ($\lambda_\odot$), and the Öpik values $U$, $\cos\theta$, $\theta$, and $\phi$ (Öpik, 1976). The 22 elements allow 231 combinations.
**Background:** Removes or replaces unassigned background radiants from the overlay plots.
**Calculate S/B:** Calculate the shower-to-background ratios and plot the ellipses (Jenniskens et al., 2016c).
**Sigma Factors:** Drop-down menus to select the standard deviations for the S/B calculations.
**Replot:** Change marker size, plot frame offset (zoom), and solar longitude beginning and end.
**B/W:** Changes the plot colors for good B/W conversion.
**CAMS:** Select among the CAMS networks when CAMS data is displayed.
**MOAT files:** Creates a file of the currently assigned radiants that can be loaded back into Moat as meteor data.
**Save Data/GUI:** Creates a data file of all displayed radiants and a `.png` image file of the GUI.

All app features are described in detail in the Moat User Manual included in the download folder.

## 3 The MOAT shower catalog

The Moat shower catalog uses shower data from CAMS (Jenniskens et al., 2016a) and the MDC Shower Database (SD) list of all showers (Jenniskens et al., 2020), with data additions and corrections made for both sources. Before release Moat was used to check the accuracy of the R.A., Decl., and $V_g$ shower data in Jenniskens (2023), and almost 500 shower entries were confirmed or corrected. Seven showers defined by an assumed $e = 1.00$ (#158, 159, 181, 793, 853, 870, and 1121) were changed to $e = 0.9999$ to prevent division by zero, and the corresponding values of $a$ and $1/a$ were added. Showers with $e > 1$ were left intact. Showers defining only a peak $\lambda_{\odot\max}$ were given an activity period of $\lambda_{\odot\max} \pm 7°$. Showers with undefined drift rates are given default $\Delta$R.A. or $\Delta$ecliptic longitude ($\Delta\lambda_g$) values of 1.0° so there is an option of applying a generic drift rate when none is defined. Ecliptic coordinates (J2000) were calculated for all showers and all angular values were confined to 0°–359.9999°.

The catalog includes showers listed in the downloaded SD list of all meteor showers; IAU numbers 1 to 1211 for a total of 979 showers. This list includes some showers that have 'removed' status. Three shower complexes with a single shower member were included (#93, 103, and 105). The remaining shower complex IAU numbers were omitted for lack of orbital elements, and their members are listed individually. Several showers listed in the catalog are radar detections and show little if any activity in video data. An Excel Worksheet version of the file is included in the app folder to allow easy editing.

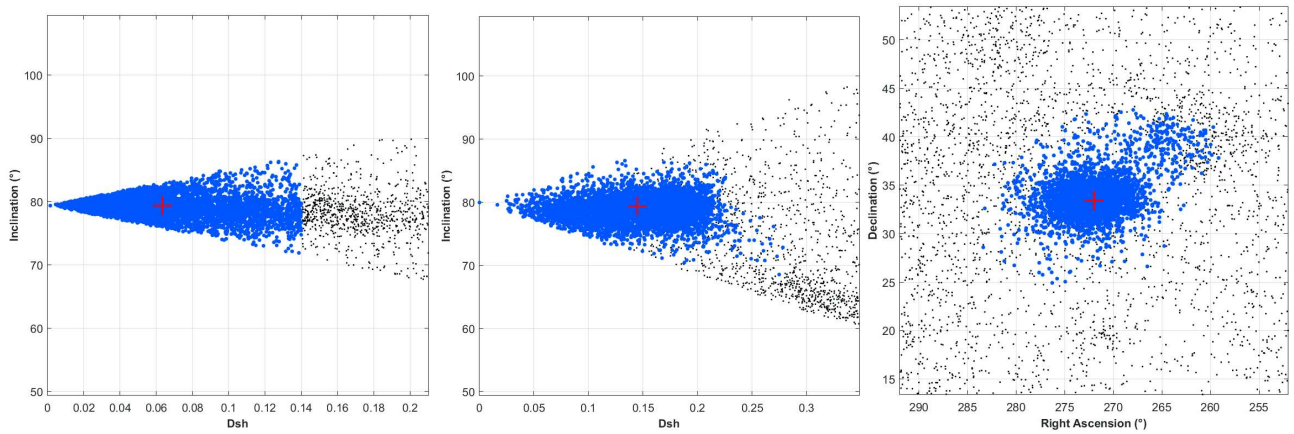


*Figure 4* – Left: Dsh results for threshold $D_c = 0.14$ before iterations; Center: Dsh results after 3 iterations seen in Figure 2, with the highest assigned radiant at Dsh $\approx 0.275 \approx D_{c_{eff}}$; Right: Dsh for $D_c = 0.275$ applied to the catalog mean Lyrid orbit. Compare to Figure 2.

Some showers in the SD are at different locations than the given R.A./Decl. coordinates, cases of which are discussed in Jenniskens (2023), and the corrected data solved many of the location problems. One location error was corrected manually for #507 UAN (Holman & Jenniskens, 2013) using Moat in Search mode. The most common error found in the SD is a displacement of data values in the $i$, $\omega$, and $\Omega$ columns, where all the correct values have been entered, but in the wrong columns. The remaining uncorrected errors manifest as showers that plot centered in the orbital element plots, but are far off center or absent from the equatorial and ecliptic plots. This is sometimes due to the choice of D function.

## 4 Using MOAT

Raising $D_c$ for a D function until the removal plot has a smooth background will theoretically identify every shower member. High thresholds usually result in a cluster in the overlay plot that is too large and begins to take in sporadic and nearby separate shower radiants, leaving an unnatural looking background in the removal plot. Using a lower $D_c$ can find a set common to the parent body, but will not identify all shower members (Jenniskens et al., 2016b).

Alternatively, a very low $D_c$ and the use of the interactive feature will reduce the cluster gradually by iteration. Clicking on a radiant in the remaining cluster will retrieve a set of orbits to choose from for the next iteration. The active D function can then be applied using the new comparison orbit. Iterating with a sufficiently low $D_c$ is useful when separating showers that are located next to each other, like #1-CAP and #692-EQA or North/South stream branches. Careful selection of comparison orbits can be used to identify and separate streamlets at different Nodes shed by different comet passes. Iterations can then be viewed individually or in combination using the Iteration Viewer.

Most of the Lyrids shown in the Figures were removed after 3 iterations using instead a rather high $D_c$ (0.14), which left a small central cluster of radiants with eccentricities $\geq 1$. The **Eccentricity Filter** removed radiants left behind due to velocity error, and the result is shown in Figure 2. A partial halo of radiants with position errors remain to the northeast and southwest.

Iterating at a threshold $D_c$ increases some of the D values of assignments made by previous iterations above $D_c$, resulting in an "effective" threshold, $D_{c_{eff}}$. The $D_{c_{eff}}$ for Figure 2 is $\sim 0.275$, seen in the center plot of Figure 4, and is almost twice the set threshold. $D_{c_{eff}}$ is not an absolute threshold like $D_c$ (left plot of Figure 4) and there are radiants with $D_{SH} < D_{c_{eff}}$ that are not assigned as part of the shower cluster. If $D_{c_{eff}}$ is applied to the initial comparison orbit as an absolute threshold without any iteration, the resulting assigned shower cluster becomes more diffuse and begins to take in the unrelated 90-Herculids (NHE) to the northwest (right plot of Figure 4). Iterating with a small $D_c$ provides a method to apply effectively larger thresholds surgically.

In Search mode Moat can be aimed at any point in the sky for any solar longitude to inspect a suspected shower radiant cluster. The orbital elements can be entered before plotting, or established by clicking on the suspect radiant cluster after Moat has plotted it. Parent body orbital elements can be entered to find matches with meteor orbits.

There are many criticisms of D criteria functions that use orbital elements in the literature including: too many dimensions, $e$ not being a dimension, violation of the triangle axiom of metric space, or singularities when $i = 0$, or $e = 0$, or $|\Omega_1 - \Omega_2| = 180°$ or $0°$. D functions that use $\Omega$ (**Dsh, Dd, Dh**) are best when used with $|\Omega_1 - \Omega_2| \leq 7$, and all D functions using orbital elements benefit from small solar longitude periods, which also translate to small $|\Omega_1 - \Omega_2|$ and to smaller variations of the elements over time. **Dst** and **Da** omit the use of $\Omega$ and are suitable for long solar longitude periods, and **Da** uses $a$ instead of $q$, suitable for asteroidal showers. D criteria results do not conclusively associate a set of meteor orbits with a common parent body. Further dynamical studies are required before the associated meteors can be considered a true shower.

## 5 Conclusion

Moat is a user friendly interactive GUI app for fast and accurate D criteria studies. Large plots show the shower in ecliptic and equatorial coordinates, and orbital element space. The Moat shower catalog includes 979 MDC showers, and Moat can be aimed at any point in the sky to examine new showers. Publicly available meteor orbit data from five major sources is included, and more meteor and shower data can be added. Moat produces text files of all results and can make image files of the plots. Ten D criteria functions are available, and can be applied iteratively. All D criteria functions have limitations and must be used carefully. Moat runs on Matlab Runtime, and both are free downloads.

## Downloading and installing MOAT and MATLAB Runtime

The Moat app and data folder is 1.53 GB (750 MB zipped), and is uploaded at Google Drive. For access to the zipped file, email the author at:
`moat.meteors@gmail.com`. Instructions for installing Matlab Runtime are at `https://www.mathworks.com/help/compiler/install-the-matlab-runtime.html`, which includes a link to the Runtime installers. Use Runtime version 9.13 for Matlab R2022b for 64-bit Windows. Since the app was compiled in Windows it will only run on that platform. Complete installation instructions are in the Moat User Manual.

## Acknowledgement

Thanks to Pete Gural for advice during development and programming, for providing the code for $D_v$, and for compiling the app. Thanks to Peter Jenniskens for providing a way to find errors in the Moat shower catalog. The author is grateful for personal communication with Toru Kanamori that made it possible for the app to load the SonotaCo SNMv3 data. Cite this paper when using Moat for published work.

## References

Asher D. J., Clube S. V. M., and Steel D. I. (1993). "Asteroids in the Taurid Complex". *Mon. Not. R. Astron. Soc.*, **264**, 93–105.

Drummond J. D. (1981). "A test of comet and meteor shower associations". *Icarus*, **45:3**, 545–553.

Holman D. and Jenniskens P. (2013). "Discovery of the Upsilon Andromedids (UAN, IAU #507)". *WGN, Journal of the International Meteor Organization*, **41:2**, 43–47.

Jenniskens P. (2008). "Meteoroid streams that trace to candidate dormant comets". *Icarus*, **194:1**, 13–22.

Jenniskens P. (2023). *Atlas of Earth's Meteor Showers*. Elsevier, Amsterdam.

Jenniskens P., Baggaley J., Crumpton I., Aldous P., Pokorny P., Janches D., Gural P. S., Samuels D., Albers J., Howell A., Johannink C., Breukers M., Odeh M., Moskovitz N., Collison J., and Ganju S. (2018). "A survey of southern hemisphere meteor showers". *Planetary and Space Science*, **154**, 21–29.

Jenniskens P., Jopek T. J., Janches D., Hajduková M., Kokhirova G. I., and Rudawska R. (2020). "On removing showers from the IAU Working List of Meteor Showers". *Planetary and Space Science*, **182**, 104821.

Jenniskens P., Nénon Q., Albers J., Gural P. S., Haberman B., Holman D., Morales R., Grigsby B. J., Samuels D., and Johannink C. (2016a). "The established meteor showers as observed by CAMS". *Icarus*, **266**, 331–354.

Jenniskens P., Nénon Q., Gural P. S., Albers J., Haberman B., Johnson B., Holman D., Morales R., Grigsby B. J., Samuels D., and Johannink C. (2016b). "CAMS confirmation of previously reported meteor showers". *Icarus*, **266**, 355–370.

Jenniskens P., Nénon Q., Gural P. S., Albers J., Haberman B., Johnson B., Morales R., Grigsby B. J., Samuels D., and Johannink C. (2016c). "CAMS newly detected meteor showers and the sporadic background". *Icarus*, **266**, 384–409. , and personal communication.

Jopek T. J. and Froeschle C. (1997). "A stream search among 502 TV meteor orbits. An objective approach.". *Astronomy and Astrophysics*, **320**, 631–641.

Jopek T. J., Rudawska R., and Bartczak P. (2008). "Meteoroid Stream Searching: The Use of the Vectorial Elements". *Earth Moon and Planets*, **102:1-4**, 73–78.

Korlević K., Šegon D., Andreić Ž., Novoselnik F., Vida D., and Skokić I. (2013). "Croatian Meteor Network Catalogues of Orbits for 2008 and 2009". *WGN, Journal of the International Meteor Organization*, **41:2**, 48–51.

Kornoš L., Koukal J., Piffl R., and Tóth J. (2014a). "EDMOND Meteor Database". In Gyssens M., Roggemans P., and Zoladek P., editors, *Proceedings of the International Meteor Conference, Poznan, Poland, 22-25 August 2013*. pages 23–25.

Kornoš L., Matlovič P., Rudawska R., Tóth J., Hajduková, M. J., Koukal J., and Piffl R. (2014b). "Confirmation and characterization of IAU temporary meteor showers in EDMOND database". In Jopek T. J., Rietmeijer F. J. M., Watanabe J., and Williams I. P., editors, *Meteoroids 2013 Conference, A.M. University, Poznań, Poland, Aug. 26-30, 2013*. pages 225–233.

Öpik E. J. (1976). *Interplanetary Encounters*. Elsevier, Amsterdam.

Rudawska R., Matlovič P., Tóth J., and Kornoš L. (2015). "Independent identification of meteor showers in EDMOND database". *Planetary and Space Science*, **118**, 38–47.

SonotaCo (2009). "A meteor shower catalog based on video observations in 2007-2008". *WGN, Journal of the International Meteor Organization*, **37:2**, 55–62.

SonotaCo (2016). "Observation error propagation on video meteor orbit determination". *WGN, Journal of the International Meteor Organization*, **44:2**, 42–45.

SonotaCo (2017). "Exhaustive error computation on 3 or more simultaneous meteor observations". *WGN, Journal of the International Meteor Organization*, **45:5**, 95–97.

SonotaCo, Masuzawa T., Sekiguchi T., Miyoshi T., Fujiwara Y., Maeda K., and Uehara S. (2021). "SNMv3: A Meteor Data Set for Meteor Shower Analysis". *WGN, Journal of the International Meteor Organization*, **49:3**, 64–70.

Southworth R. B. and Hawkins G. S. (1963). "Statistics of meteor streams". *Smithsonian Contributions to Astrophysics*, **7**, 261–285.

Steel D. I., Asher D. J., and Clube S. V. M. (1991). "The structure and evolution of the Taurid complex". *Mon. Not. R. Astron. Soc.*, **251**, 632–648.

Valsecchi G. B., Jopek T. J., and Froeschlé C. (1999). "Meteoroid stream identification: a new approach - I. Theory". *Mon. Not. R. Astron. Soc.*, **304:4**, 743–750.

Vida D., Gural P. S., Brown P. G., Campbell-Brown M., and Wiegert P. (2020). "Estimating trajectories of meteors: an observational Monte Carlo approach - I. Theory". *Monthly Notices of the Royal Astronomical Society*, **491:2**, 2688–2705.

Vida D., Šegon D., Gural P. S., Brown P. G., McIntyre M. J. M., Dijkema T. J., Pavletić L., Kukić P., Mazur M. J., Eschman P., Roggemans P., Merlak A., and Zubović D. (2021). "The Global Meteor Network - Methodology and first results". *Monthly Notices of the Royal Astronomical Society*, **506:4**, 5046–5074.

*Handling Editor:* Javor Kac

# The Interpretation of Complex Areas of Meteor Shower Radiants

*Yasuo Shiba*[1]

This paper is a supplement to add two points for my recent paper (Shiba, 2023) which is the Halley type and long-period meteor showers luminous height research. One is the detailed data for five newly identified meteor showers. The second is the complexity of meteor showers' by contrasting my identifications and those in the IAU MDC. In conclusion, I propose a new meteor shower identifying method exploitation that is an assessment of the radiant or orbit density in space, rather than the "D criterion", as the focus on the meteor orbit differences amount.

Received 2023 September 29

## 1 Introduction

The method used to determine whether individual meteors belong to any meteor showers is described below. Initially, two types of radiant distribution charts were drawn for 10 degree solar longitude intervals. One shows right ascension vs declination of meteors' radiants; the second shows individual meteors' radiants (ecliptic longitude – solar longitude, $\lambda - \lambda_{\odot}$) vs ecliptic latitude ($\beta$). Regions with radiant concentrations in the charts were identified, but any meteors within them that had vastly extreme different geocentric velocity meteors were removed. The orbit differences assessment value "Dd" (Drummond, 1980) calculation compared the orbits of the selected meteors with their mean orbit. Meteors with exceptionally large Dd values were removed from the meteor shower membership. Finally, those meteors still remaining are considered to be members of the meteor shower. If I found concentrated regions over 10-degree solar longitude and implied continuous radiant positions and drift, that were decided as identical meteor showers.

## 2 New meteor showers

The average data for the new meteor showers is shown in Table 1 and all radiant point distributions are shown in Figures 1-5.

Table 1 headers are below.
code: meteor shower code,
Activi: type of activity,
$\lambda_{\odot}$: mean solar longitude (J2000; deg),
$\lambda_{\odot}$b: activity beginning,
$\lambda_{\odot}$e: activity ending,
R.A., Decl.: corrected radiant position (J2000.0),
Δ R.A., Δ Decl.: radiant point drift per solar longitude,
$\lambda$: ecliptic longitude of the shower radiant (J2000),
$\lambda - \lambda_{\odot}$, $\beta$: ecliptic latitude of the shower radiant (J2000),
$\Delta\lambda$, $\Delta\beta$: radiant drift for ecliptic coordinate,
$V_g$: geocentric velocity,
$\Delta V_g$: velocity increase per solar longitude,
$n$: meteors number,
$a$: orbit semi major axis,
$q$: perihelion distance,
$e$: eccentricity,

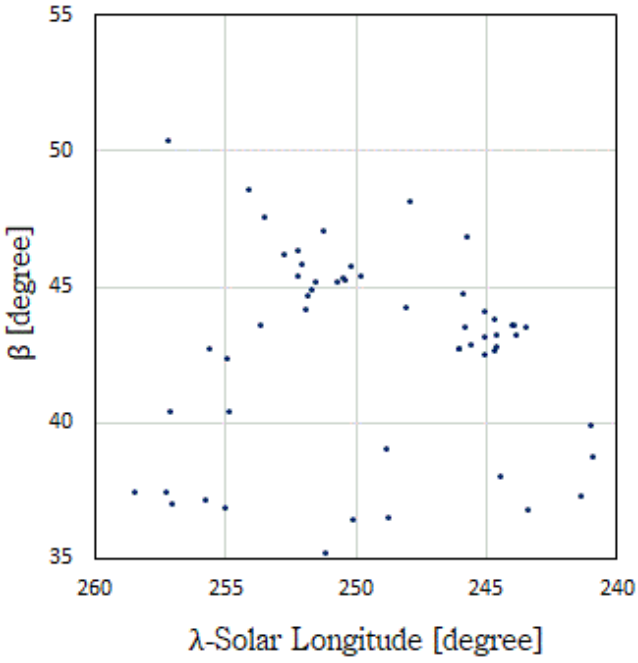


*Figure 1* – M2023-F1 radiant distribution ($\lambda_{\odot}$ = 237.6–242.4°). The shower on the right side is #488 NSU.

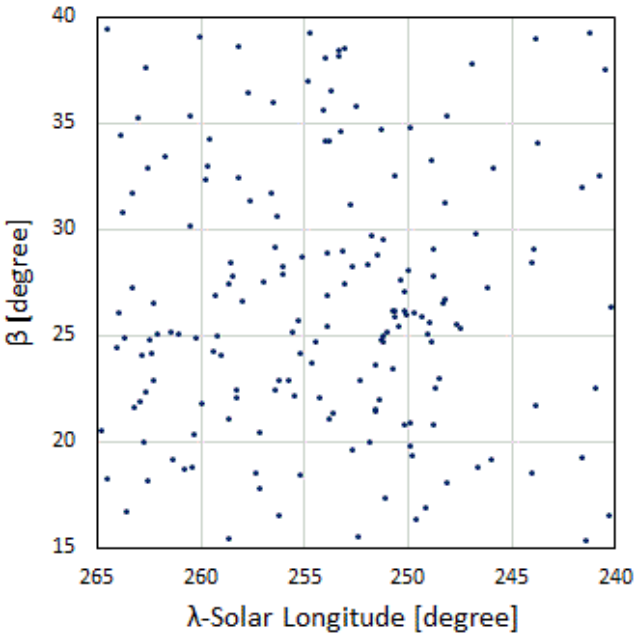


*Figure 2* – M2023-F2 radiant distribution ($\lambda_{\odot}$ = 56.3–78.9°).

[1]SonotaCo Network
Email: kqc43540@biglobe.ne.jp

IMO bibcode WGN-515-shiba-interpretation
NASA-ADS bibcode 2023JIMO...51..118S

*Table 1* – New identified meteor showers.

| Code | Activi | $\lambda_\odot$ | $\lambda_\odot$b | $\lambda_\odot$e | R.A. | Decl. | ΔR.A. | ΔDecl. | $\lambda$ | $\lambda - \lambda_\odot$ | $\beta$ | $\Delta\lambda$ | $\Delta\beta$ | $V_g$ | $\Delta V_g$ |
|---|---|---|---|---|---|---|---|---|---|---|---|---|---|---|---|
| M2023-F1 | annual | 239.24 | 237.64 | 241.35 | 155.79 | 59.71 | 1.34 | −0.45 | 130.79 | 251.54 | 45.24 | 1.15 | −0.03 | 55.02 | 0.09 |
| M2023-F2 | annual | 67.3 | 56.33 | 78.86 | 311.78 | 9.11 | 0.84 | 0.19 | 317.02 | 249.73 | 25.91 | 0.95 | −0.06 | 63.25 | −0.03 |
| M2023-F4 | annual | 277.01 | 274.58 | 278.61 | 164.34 | 54 | 1.49 | −0.13 | 140.44 | 223.42 | 42.79 | 1.11 | 0.34 | 47.99 | 0.02 |
| M2023-F5 | annual | 265.1 | 260.49 | 269.86 | 164.34 | 20.47 | 1.09 | −0.34 | 157.65 | 252.55 | 12.74 | 1.1 | 0.09 | 68.01 | −0.04 |
| M2023-F3 | annual | 22.11 | 9.65 | 36.63 | 266.28 | −15.93 | 0.85 | −0.02 | 266.39 | 244.29 | 7.34 | 0.83 | −0.01 | 65.93 | −0.06 |

| Code | $n$ | $a$ | $q$ | $e$ | $p$ | peri | node | incl | Mag | Hb | He | elev | Dd |
|---|---|---|---|---|---|---|---|---|---|---|---|---|---|
| M2023-F1 | 14 | 13.4 | 0.894 | 0.933 | 48.9 | 216.6 | 239.2 | 99.6 | −0.97 | 113.8 | 99.3 | 41.1 | 0.022 |
| M2023-F2 | 22 | 26.8 | 0.787 | 0.971 | 139 | 236.9 | 67.3 | 130.9 | −1.81 | 109.7 | 90.6 | 48.1 | 0.05 |
| M2023-F4 | 13 | 19.3 | 0.609 | 0.968 | 85.1 | 256.9 | 277 | 79.4 | −1.42 | 107.4 | 89.1 | 48.5 | 0.033 |
| M2023-F5 | 25 | 10.6 | 0.744 | 0.93 | 34.5 | 240.4 | 265.1 | 155.5 | −1.04 | 111 | 95.9 | 52.9 | 0.043 |
| M2023-F3 | 31 | 13.3 | 0.534 | 0.96 | 48.3 | 267.3 | 22.1 | 163.9 | −1.42 | 111.6 | 95.7 | 31.7 | 0.066 |

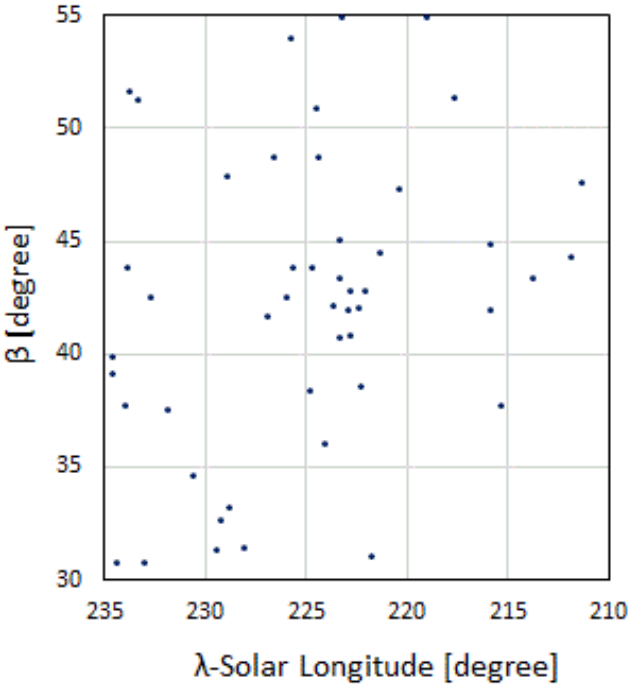


*Figure 3* – M2023-F4 radiant distribution ($\lambda_\odot$ = 274–279°).

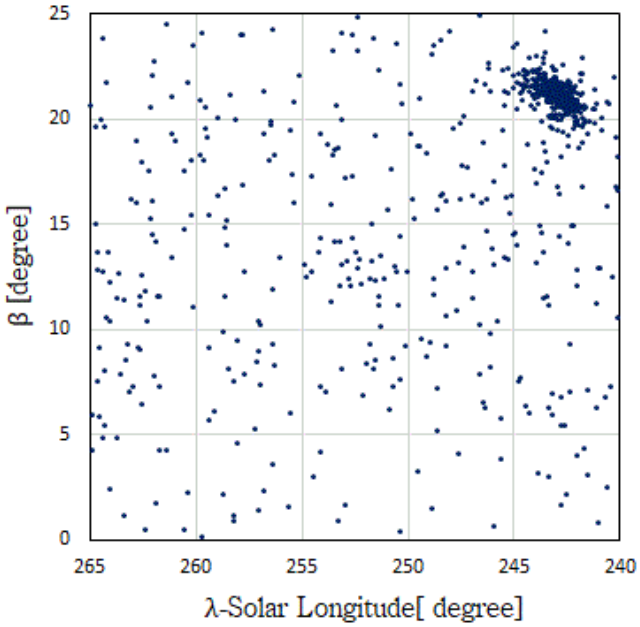


*Figure 4* – M2023-F5 radiant distribution ($\lambda_\odot$ = 260 ∼ 270°). The shower on the upper right is #20 COM.

*p*: period,
peri: argument of perihelion,
node: ascending node,
incl: inclination,
Mag: mean luminous magnitude,
Hb: mean start height,
He: mean end height,
elev: mean radiant point elevation angle, and
Dd: mean D criterion (Drummond, 1980).

In Figures 1–5, the horizontal axis is drawn as the (radiant ecliptic longitude minus the solar longitude) and the vertical axis is radiant ecliptic latitude.

M2023-F3 is same as #958 SXS (Amaral et al., 2018) on IAU MDC but that data was already removed from working list for 2023.

## 3 The complexity of meteor showers

The contrast between my allocated meteor showers (Shiba, 2023) and the IAU MDC is shown in Table 2. “Synonym” indicates that showers were judged

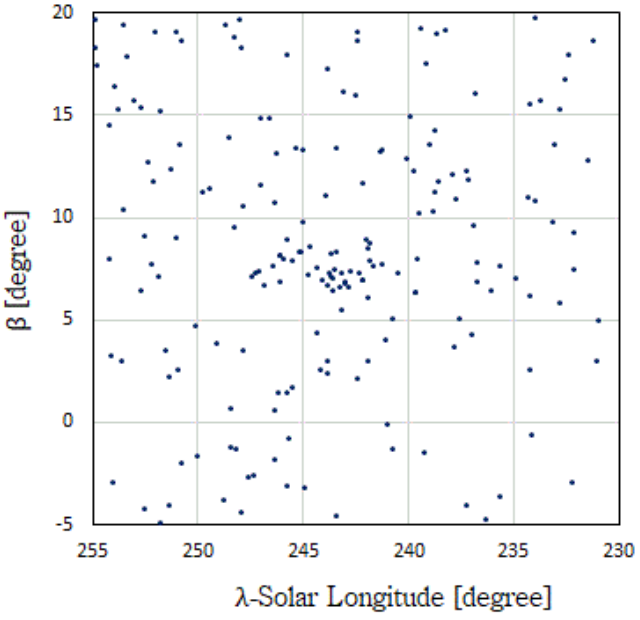


*Figure 5* – M2023-F3 = #958 SXS radiant distribution ($\lambda_\odot$ = 10–40°).

*Table 2* – Meteor shower name comparison: Shiba (2023) and IAU MDC.

| | Shiba, 2023 | | IAU MDC | | |
|---|---|---|---|---|---|
| # | Code | Meteor shower name | Synonym | Pre-Shower | Post-Shower | Simillar showers |
| 7 | PER | Perseids | | | | #444 ZCS |
| 8 | ORI | Orionids | #1198 XRO | #226 ZTA[*1] | | #718 XGM |
| 13 | LEO | Leonids | | #481 OML | | |
| 16 | HYD | sigma Hydrids | | | | **#246 AMO**, #1196 ZCM |
| 19 | MON | December Monocerotids | | | #1098 EMI | |
| 20 | COM | Comae Berenicids | #32 DLM[*2], #90 JCO, #499 DDL[*3], **#506 FEV** | | | |
| 27 | KSE | kappa Serpentids | | | | #836 ABH, #839 PSR |
| 31 | ETA | eta Aquariids | | | #667 JTP | |
| 40 | ZCY | zeta Cygnids | **#348 ARC**[*4], #409 NCY | | | #350 MAL |
| 81 | SLY | September Lyncids[*5] | #705 UYL | | | |
| 175 | JPE | July Pegasids | #522 SAP, #462 JGP[*6] | | #1075 AGP | #577 FPI, #829 JSP |
| 183 | PAU | Piscis Austrinids | | | | #503 NNA[*7] |
| 187 | PCA | psi-Cassiopeiids | | | | #550 KPC |
| 190 | BPE | beta-Perseids | #793 MPR | | | |
| 191 | ERI | eta Eridanids | #598 TCT | | **#337 NUE** | #430 POR, #738 RER |
| 206 | AUR | Aurigids | | #736 XIP | | #918 TAG |
| 208 | SPE | September epsilon Perseids | #874 PXS | | #717 LAU | #553 DPE, #1134 PIE |
| 246 | AMO | alpha Monocerotids | #1196 ZCM | | | |
| 250 | NOO | November Orionids | | | | #253 CMI |
| 319 | JLE | January Leonids | | | | #1190 JZL |
| 331 | AHY | alpha-Hydrids | | | | #398 DCM |
| 335 | XVI | December chi Virginids | #1117 NEV | | | |
| 337 | NUE | nu Eridanids | #430 POR[*8] | | | **#191 ERI**, #1142 SNT |
| 339 | PSU | psi Ursae Majorids | | | | #573 TLM |
| 340 | TPY | theta Pyxidids[*9] | #844 DTP | | | **#512 RPU**, #498 DMH |
| 372 | PPS | phi Piscids | #414 ATR, #667 JTP, #1112 UPI | | #693 ANP | #190 BPE, #688 BTR, #547 KAP |
| 394 | ACA | alpha Canis Majorids | #559 MCB | | | |
| 411 | CAN | c Andromedids | #507 UAN[*10] | | | #1068 TPE |
| 424 | SOL | September-October Lyncids | #81 SLY[*11] | | | |
| 425 | PSA | psi Aurigids | #613 TLY | | | #81 SLY |

[*1] Same as only Jenniskens, 2006 (Removed).
[*2] #32 DLM (Kashcheev & Lebedinets, 1967) is differ.
[*3] Removed meteor shower (a part of COM).
[*4] #348 ARC is better to remove from established list and set on #40 ZCY.
[*5] #81 SLY come under only (Table 5) of the sourcebook.
[*6] Right ascension of IAU MDC (Kornoš et al., 2014) will mistake and (Rudawska & Jenniskens, 2014) is Removed meteor shower.
[*7] #503 NNA on IAU MDC velocity data is lack.
[*8] Removed meteor shower ($N = 3$).
[*9] #340 TPY (Jenniskens et al., 2016) is better to set on #498 DMH.
[*10] #507 UAN come under only the (Holman and Jenniskens, 2013) describe.
[*11] #81 SLY come under only (Table 6) of the sourcebook.

to be the same meteor shower. "Pre-Shower" indicates that there is a continuous previous radiant position taking into account the radiant drift, but there is a gap or a difference in character existing between the two meteor showers that provide a reason for independent meteor showers. "Post-Shower" is inverse position of Pre-showers. "Closed showers" indicates radiant position differences smaller than about 5-degree and so this make it easy to cause confusion meteor showers that are individual meteors are easy to overlap.

*Table 2* – Meteor shower name comparison: Shiba (2023) and IAU MDC — continued from previous page.

| Shiba, 2023 | | | IAU MDC | | | |
|---|---|---|---|---|---|---|
| # | Code | Meteor shower name | Synonym | Pre-Shower | Post-Shower | Simillar showers |
| 428 | DSV | December sigma Virginids | #500 JPV, #513 EPV, #1124 HTV | | #614 JOS | #731 JZB |
| 439 | ASX | alpha Sextantids | #483 NAS[*12] | | #493 DEC | |
| 480 | TCA | tau Cancrids | #481 OML[*13], #654 PHC, #1114 SGC | | | |
| 488 | NSU | November sigma Ursae Majorids | #527 UUM | | | #622 PUA, M2023-F1 |
| 493 | DEC | December epsilon Craterids | #729 DCO | #439 ASX | #101 PIH | #1095 EPX, #1159 CVI |
| 494 | DEL | December Lyncids | #1049 DIU | | | #578 TUM |
| 498 | DMH | December mu Hydrids | #567 XHY, #1123 FFH | | #888 SCV, #1160 JBH | #340 TPY |
| 502 | DRV | December rho Virginids | #1116 NFL | | | |
| 512 | RPU | rho Puppids | | | | #340 TPY |
| 514 | OMC | omega Capricornids | #597 TTS | | | |
| 523 | AGC | August gamma Cepheids | | | | #701 BCE |
| 530 | ECV | eta Corvids | #1126 SOV, #601 ICT[*14] | | | #540 TCR |
| 533 | JXA | July xi Arietids | #1113 SJA | | | |
| 545 | XCA | xi Cassiopeiids | #1077 PIC | | | |
| 549 | FAN | 49 Andromedids | | #507 UAN[*15] | | #185 DBA |
| 558 | TSM | 27-Monocerotids | #245 NHD[*16] | | | #227 OMO[*17] |
| 563 | DOU | December omega Ursae Majorids | #1122 UMN | | | #565 FUM |
| 569 | OHY | omicron Hydrids | | | | #316 BHD[*18] |
| 570 | FBH | February beta Herculids | | #594 RSE | | |
| 571 | TSB | 26 Bootids | #859 MTB | | | |
| 593 | TOL | 28 Lyncids | | | #722 FLE | |
| 722 | FLE | 15 Leonids | #1118 MLT | #593 TOL | | |
| 862 | SSR | 16-Scorpiids | #968 UOD[*19] | | | |
| 884 | NBP | 15 Leonids | | | | #1119 LAV, #1162 DPV |
| 889 | YOP | Y Ophiuchids | | | #890 ESU | |
| 893 | EOP | eta Ophiuchids | | | | #652 OSP |
| 894 | JMD | June mu-Draconids | | | | #88 ODR[*20] |
| 1119 | LAV | December lambda Velids M2023-F5 | #1162 DPV | | | #443DCL, #566 BCF |

[*12] Removed meteor shower(Duplicate of #439 ASX).
[*13] #481 OML is pre-shower of #13 LEO and close to after half of #480 TCA.
[*14] #601 ICT is the north part of the initial stage activity.
[*15] #507 UAN come under only (Jenniskens, 2016).
[*16&17] Removed meteor shower.
[*18] #316 BHD is some data lacked.
[*19] Removed meteor shower.
[*20] #88 ODR come under only (Jenniskens et al., 2016).

The more complex radiant regions for four samples are shown in (Figures 6-9). The light blue dot is every radiant during the drawn solar longitude duration. The green circles are IAU MDC website catalogued radiant positions with additional description of the meteor shower name code. Plot (a) is (ecliptic longitude – solar longitude, $\lambda - \lambda_\odot$) vs ecliptic latitude ($\beta$; plot (b) is solar longitude ($\lambda_\odot$) vs (ecliptic longitude – solar longitude, $\lambda - \lambda_\odot$); plot (c) is solar longitude ($\lambda_\odot$) vs ecliptic latitude ($\beta$); and plot (d) is solar longitude ($\lambda_\odot$) vs geocentric velocity ($V_g$).

## 3.1 #20 COM region

In Figure 6, small red triangles were interpreted as belonging to the #20 COM radiant (Shiba, 2023). #499 DDL is already integrated to #20 COM and deleted from the working list. The similarity of data for #20 COM and #32 DLM is described (Kashcheyev & Lebedinets, 1967: $\lambda_\odot = 261.7°, \lambda - \lambda_\odot = 251.44°$), which suggests deleting one of them. #32 DLM (Jenniskens, 2006: $\lambda_\odot = 262.2°$; Molau & Rendtel, 2009: $\lambda_\odot = 268°$) is understood to go into #20 COM by Figure 6. The position of #20 COM (Molau & Rendtel, 2009: $\lambda - \lambda_\odot = 263.61°$) is different but the reason why

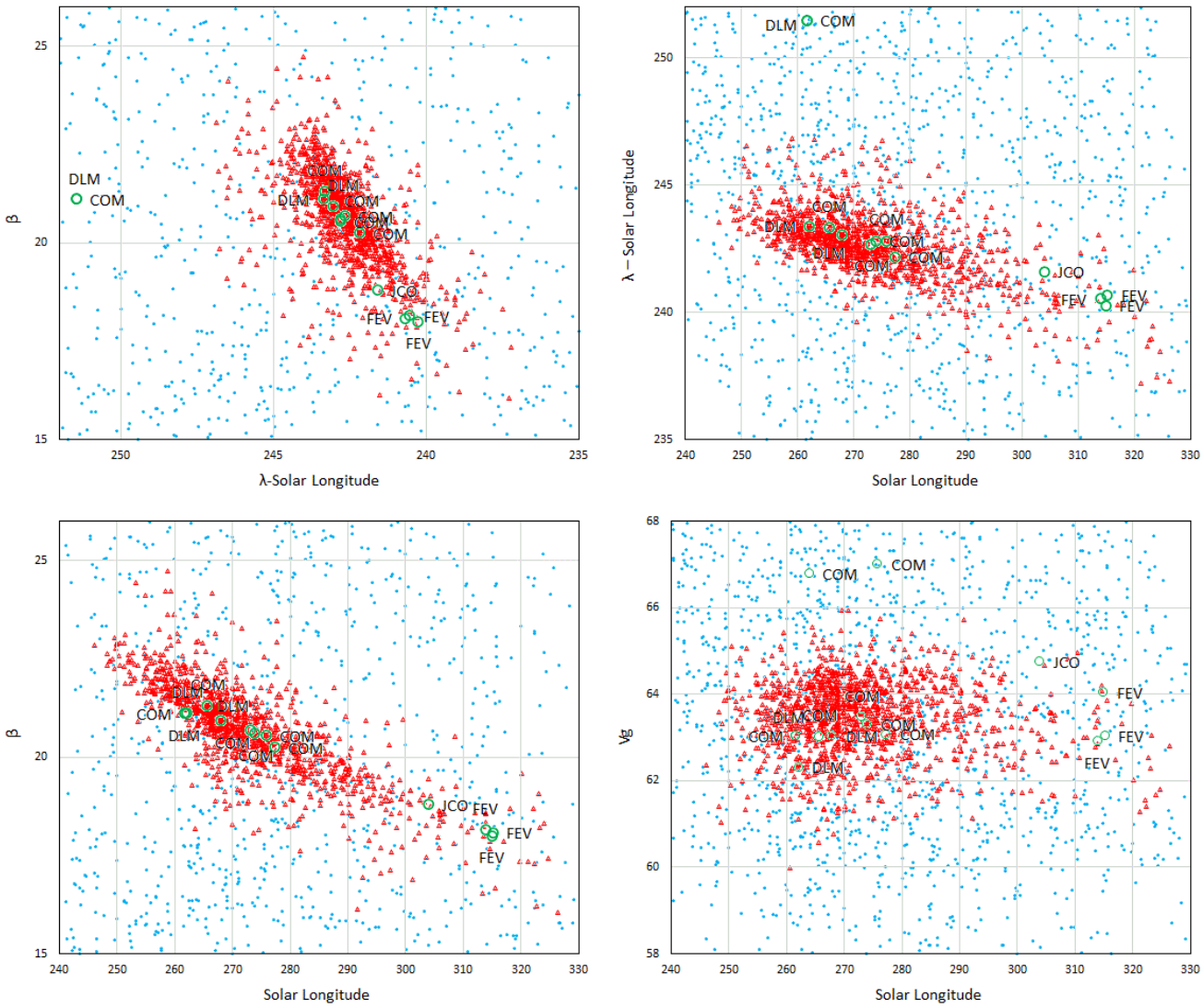


*Figure 6* – #20 COM region.

is unknown. This difficulty of comprehension for this region has already been described in Koseki (2011).

#90 JCO and #506 FEV are the final stage of #20 COM. These meteor showers were determined to be a continuation of the meteor activity of #20 COM but differ sufficiently from the mean #20 COM orbit in their D criterion (Dd > 0.25) value. Many similar combinations of meteor showers exist: (#40 ZCY – #348 ARC), (#58 TSM – #245 NHD (removed)), (#191 ERI – #598 TCT), (#208 SPE – #717 LAU), (#335 XVI – #1117 NEV), (#372 PPS – #667 JTP), (#428 DSV – #1124 HTV), (#480 TCA – #645 PHC), (#530 ECV – #1126 SOV). These pairs are determined to be different meteor showers by the D criterion but their continuation of meteor activity gives the appearance of a single meteor shower. This kind of problem has already been considered in Moorhead (2019).

## 3.2 #439 ASX to #493 DEC region

In Figure 7, small red triangles were interpreted as #439 ASX and purple square is #493 DEC (Shiba, 2023). I decided to divide these into two meteor showers because the activity in Figure 7 was supposed to decrease at about $\lambda_\odot = 250°$. However this is doubtful. The activity was found to also show small decreases at about $\lambda_\odot = 230°$ and 265°. In contrast, it is possible to interpret it as one long-duration meteor shower. If you split this activity at $\lambda_\odot = 265°$ , then #729 DCO is the final active part of this meteor activity. #483 NAS was already integrated to #439 ASX as the same meteor shower.

This four-month continually-active meteor shower gives us a difficult problem to resolve. Do we classify it as single meteor shower or divide it up into several meteor showers (accompanied by some rational justification)?

## 3.3 #372 PPS region

In Figure 8, small red triangles were interpreted as belonging to #372 PPS. This active region appears at the end position of #31 ETA after solar longitude 70 degrees. #667 JTP is the initial stage of this region and D criterion value from #372 PPS mean orbit indicates it to be another independent meteor shower, but I treated it as a continuation of the same meteor shower. In contrast, a gap exists between the #31 ETA and #667 JTP locations. The #372 PPS radiant area disperses after $\lambda_\odot = 105°$, thereby it may be recognised as

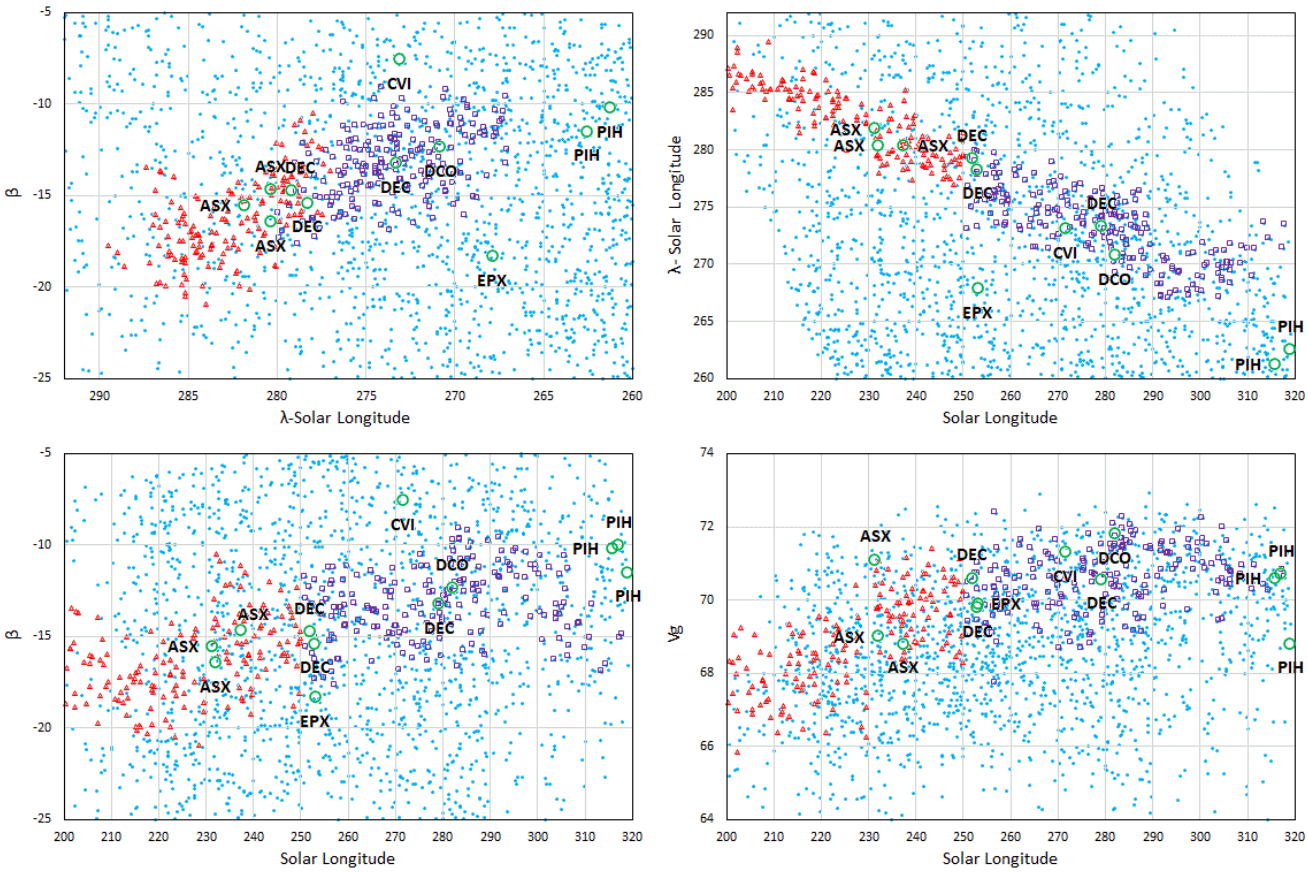


*Figure 7* – #439 ASX, #493 DEC region.

some separate meteor shower. Alternatively, a different meteor shower allocation may arise because characteristics are varying and the radiant area is dispersed. I interpreted #414 ATR and #1112 UPI as one continuous meteor activity in the broad #372 PPS radiant space. On the other hand, #688 BTR and #547 KAP were judged to be independent meteor showers because of *beta* differences. For #190 BPE, previous research was inconclusive, but I interpreted sparse radiants existing about 10 degrees the east of #372 PPS before Perseid maximum. On the continuous position of after #372 PPS, the #693 ANP at solar longitude 149 degrees and #1137 AMP at 155.8° are recorded in the IAU MDC. Activity from these regions may continue until about solar longitude 180 degrees.

Meteor showers that are possibly in a transient stage area towards the sporadic background, like #372 PPS, are difficult to recognise as meteor showers. In the near-apex direction, it is possible for this problem to occur as there are many overlapping many sporadic meteors.

### 3.4 #512 RPU, #340 TPY, #498 DMH region

In Figure 9 small purple squares are #512 RPU, small red triangles are #340 TPY, and orange diamonds are #498 DMH. The three meteor showers are adjacent but can be clearly separated. #844 DTP is presumed to be the same as #340 TPY, however #340 TPY (Jenniskens et al., 2016: $\lambda_{\odot} = 264°$, $V_g = 62.3$ and 63.2 km/s) is the same as #498 DMH. #1123 FFH is a part of #498 DMH distributions and thus these showers indicate a single meteor shower. #967 XHY is also presumed to be the ending part of #498 DMH. #888 SCV and #1160 JBH are considered to be the same meteor shower and can be judged to be separated in position from #498 DMH.

Close to #498 DMH is #340 TPY whose meteor has a small D criterion value to the #498 DMH mean orbit (Dd = 0.064). This gives the anomalous result that this meteor belongs to two meteor showers simultaneuously. We must pay attention to similar confusion when using the D criterion on closed meteor shower positions for two or more meteor showers.

## 4 Suggestions

Since the original D criterion development (Southworth & Hawkins, 1963), the D criterion has made a tremendous contribution to meteor shower assignment. Its objective and quantitative technique has offered the potential of excellent science. In order to enhance the quality of its results, many researchers have iterated its improvement (Jopek et al., 2008; Sokolova et al., 2014). However, the D criterion technique contains an unresolved problem in the case of single meteor shower being split into two or more meteor shower or one meteor being assigned to two or more meteor showers.

A new concept technique development is needed to resolve this unresolved D criterion problem. Instead of the D judgment, which quantitatively evaluates the similarity of meteor orbits, we quantitatively evaluate the

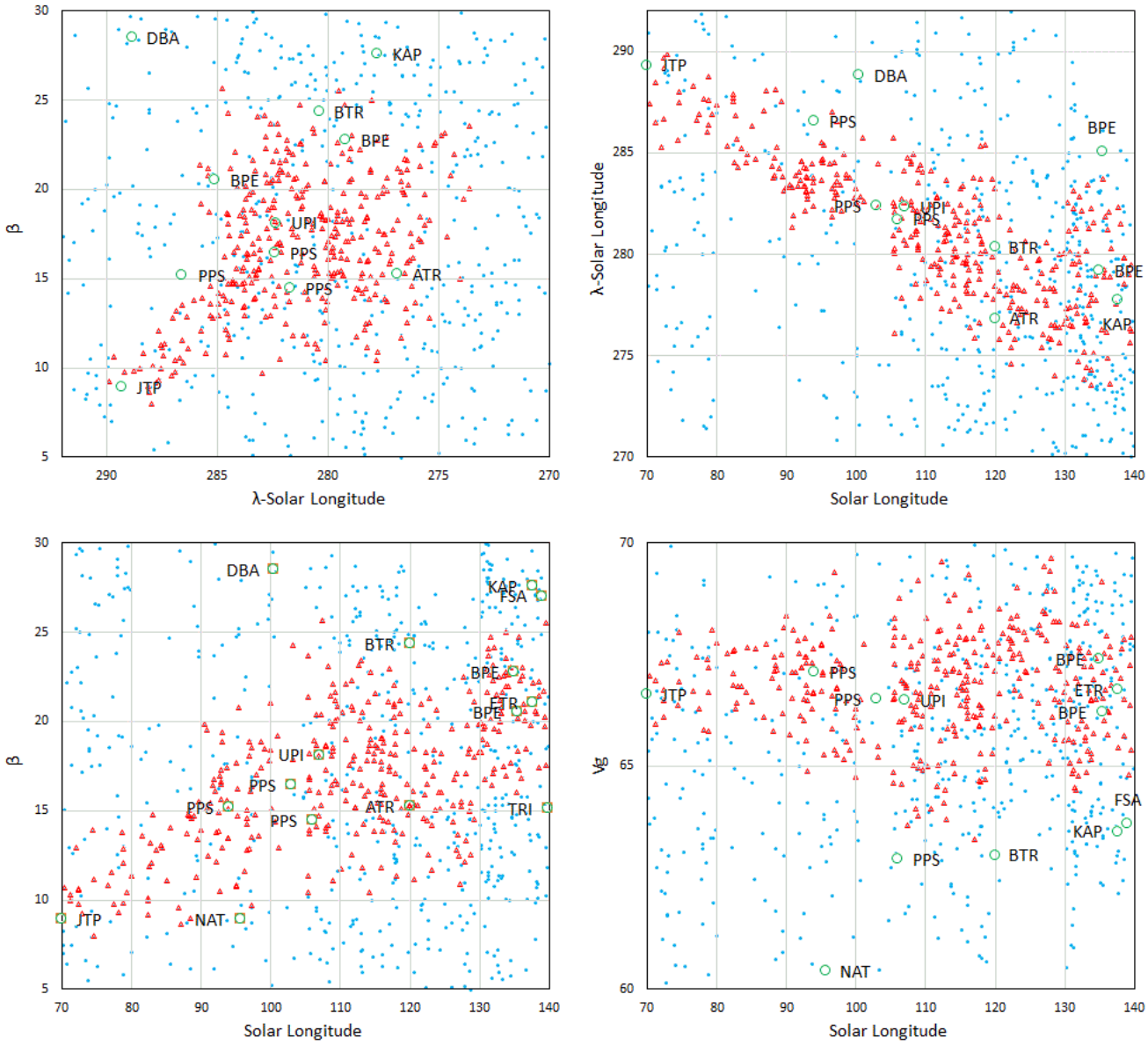


*Figure 8* – #372 PPS region.

areas with high meteor density in the four-dimensional space of the meteor's radiant point, velocity, and solar longitude (R.A., Decl, $V_g$, Solar Longitude). An objective criterion would be promising. This can also be replaced by selecting a region where the spatial density of the orbital distribution in the five-dimensional space ($e$, $q$, $\omega$, $\Omega$, $i$) of the meteor orbit is high. The expected future combination with accumulated TV and radio meteor orbit data will bring us semi-automatic meteor shower detection.

## Acknowledgements

Mr. Javor Kac gave me valuable information on IAU MDC data. I am very grateful to him.

## References

Amaral L. S., Bella C. A. P. B., Trindade L. S., Zurita M. L. P. V., Silva G. G., Domingues M. W. S., Poltronieri R. C., Faria C. J. L., and Jung C. F. (2018). "A Search Method for Meteor Radiants". *WGN, Journal of the International Meteor Organization*, **46:6**, 191–197.

Drummond J. D. (1980). "On the meteor/comet orbital discriminant D.". In Gott P. F. and Riherd P. S., editors, *Southwest Regional Conference for Astronomy and Astrophysics, 5*, volume 5. pages 83–86.

Jenniskens P. (2006). *Meteor Showers and their parent comets*. Cambridge.

Jenniskens P., Nénon Q., Gural P. S., Albers J., Haberman B., Johnson B., Holman D., Morales R., Grigsby B. J., Samuels D., and Johannink C. (2016). "CAMS confirmation of previously reported meteor showers". *Icarus*, **266**, 355–370.

Jopek T. J., Rudawska R., and Bartczak P. (2008). "Meteoroid Stream Searching: The Use of the Vectorial Elements". *Earth Moon and Planets*, **102:1-4**, 73–78.

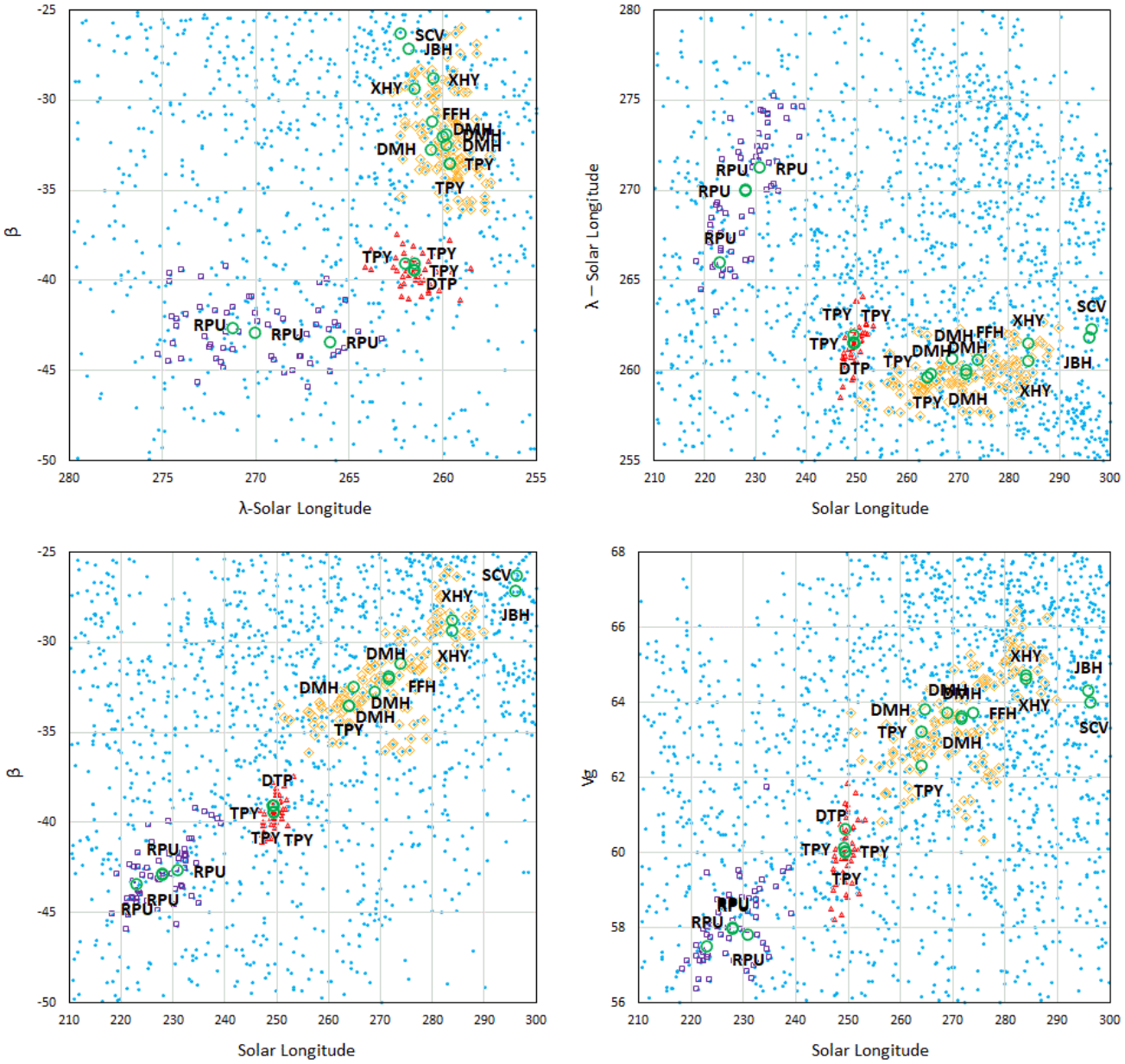


*Figure 9* – #512 RPU, #340 TPY, #498 DMH region.

Kashcheyev B. L. and Lebedinets V. N. (1967). "Radar studies of meteors". *Smithsonian Contributions to Astrophysics*, **11**, 183–199.

Koseki M. (2011). "Comae Berenicids and related activities". *WGN, Journal of the International Meteor Organization*, **39:6**, 159–166.

Molau S. and Rendtel J. (2009). "A Comprehensive List of Meteor Showers Obtained from 10 Years of Observations with the IMO Video Meteor Network". *WGN, Journal of the International Meteor Organization*, **37:4**, 98–121.

Moorhead A. V. (2019). "Meteor shower activity profiles and the use of orbital dissimilarity (D) criteria". *WGN, Journal of the International Meteor Organization*, **47:5**, 134–138.

Shiba Y. (2023). "Halley Type and Long Period Meteor Shower Luminous Altitude Characteristics". *WGN, Journal of the IMO*, **51:4**, 93–108.

Sokolova M., Nefedyev Y., and Andreev A. (2014). "Analysis of the D-criteria". In *European Planetary Science Congress*, volume 9. pages EPSC2014–275.

Southworth R. B. and Hawkins G. S. (1963). "Statistics of meteor streams". *Smithsonian Contributions to Astrophysics*, **7**, 261–285.

*Handling Editors:* Javor Kac and Tracie Heywood

# Thatcher's Haunting: Other ghosts appear

*David Holman*[1], *Peter Jenniskens*[2]

At the time of comet Thatcher's April Lyrid shower (LYR, IAU #6), other nearby showers are detected in low-light video observations that may, or may not, have the same source. The Meteor Orbit Association Tool v1.0 (MOAT) MATLAB app was used to find clusters, create plots, and analyze the data. Here, we report on a shower provisionally called omega-Herculids (code OHE), a loose cluster of radiants that forms 30° to the south-west of the mean April Lyrids radiant. This activity has been observed before but reported inaccurately as the kappa-Serpentids. We observed the OHE shower to be active from solar longitude 22° to 33°. The kappa-Serpentids are active during solar longitude 6° to 20°. The $D_R$ results indicate that the OHE may have a common parent body with LYR. Also, M2023-O1 is the MDC designation for a newly recognized compact cluster of radiants that appears 5° south of the mean LYR radiant and peaks just after the first LYR radiants appear. We provisionally name this shower the nu-Herculids (code NUH). The NUH appear not related to comet Thatcher.

Received 2023 August 16

## 1 Introduction

Since the publication of "Thatcher's Ghost" (Jenniskens & Haberman, 2013) much more data has accumulated from the Cameras for Allsky Meteor Surveillance (CAMS) low-light video camera network, the European viDeo Meteor Observation Network Database (EDMOND), the SonotaCo Network, and the Global Meteor Network (GMN) (e.g., Jenniskens et al., 2011, 2018; Kornoš et al., 2014a,b; SonotaCo 2009, 2016, 2017; SonotaCo et al., 2021; Vida et al., 2020, 2021; respectively).

The Meteor Orbit Association Tool v1.0 (Moat) (Holman, 2023) was used to examine this new data around the April Lyrid (LYR) radiant direction and activity period in solar longitude intervals of one degree. Previously, this region was known to contain the following showers: the April Lyrids (LYR), nu-Cygnids (NCY), phi-Serpentids (PSR), 90-Herculids (NHE), and the April 102-Herculids (AHE).

Here, we report on two newly identified showers with radiants near that of LYR during April and early May and discuss their possible association with comet Thatcher.

## 2 Methods

Newly identified clusters were extracted with the Meteor Orbit Association Tool v1.0 (Moat). This is a Matlab application that can be used to find clusters, create plots, and analyze the data. Clusters were extracted using the D criteria function $D_N$ (Valsecchi et al., 1999) at low thresholds to recover a subset of the cluster. Initially a cluster member was selected as the comparison orbit for $D_N$ and the resulting medians were then used as the next comparison orbit for $D_N$ . This was repeated until the members selected by $D_N$ and their medians stabilized.

[1]5990 SE King Rd. #41, Milwaukie, OR 97222 USA.
Email: daveh@lmi.net
[2]SETI Institute, 339 Bernardo Ave, Mountain View, CA 94043, USA.

IMO bibcode WGN-515-holman-thatcher
NASA-ADS bibcode 2023JIMO...51..126H

To investigate whether the observed clusters may have a common source, a different D criteria function $D_R$ , using near-invariants (Valsecchi et al., 1999), was used to link meteor orbits that have undergone significant secular perturbation from the Kozai resonance over long periods of time, but that have not experienced close gravitational encounters. This D criteria function is based on the near-invariants $U$, the unperturbed geocentric velocity vector, and $\cos\theta$, where $\theta$ is the angle between $U$ and the direction of Earth's motion (Öpik, 1976).

## 3 The omega-Herculids (OHE)

The kappa-Serpentids (KSE, IAU #27) were initially identified by McCrosky & Posen (1959) from three photographed orbits with R.A. = 226–232°, Decl. = +16–20° (B1950.0) and speed $V_g$ = 42.0–46.7 km/s during the solar longitude interval from 12 to 18°. Since that time, the shower was confirmed from low-light video observations as being active in early April from 6° to 20° solar longitude.

Diffuse activity from this same radiant area during later solar longitudes has since been detected independently by Shiba (2023) and Jenniskens (2023) just next to the compact shower PSR, IAU #839 (Jenniskens et al., 2018). These detections were misclassified as being from the kappa-Serpentids (KSE). Here, we call this activity the omega-Herculids (code OHE) and report the shower details with a sample of the observed data.

The 142 sampled OHE meteors are in a Halley type orbit, or possibly a long period comet orbit if there is measurement error, with a median Tisserand parameter with respect to Jupiter ($T_J$) of +0.368 and a median orbital period of ∼ 63 years. When the sample is examined in small time intervals, the shower is active from solar longitude 25.06° – 32.68° with a peak at 29.4°. Taken together, the shower is active from solar longitude 22° – 33°. During 2007 to 2023, the OHE returned every year, but was not detected in 2008, perhaps due to weather.

Figure 1, Right, shows the results of $D_R$ on the mean LYR orbit using a threshold of $D_c$ = 0.0207, which

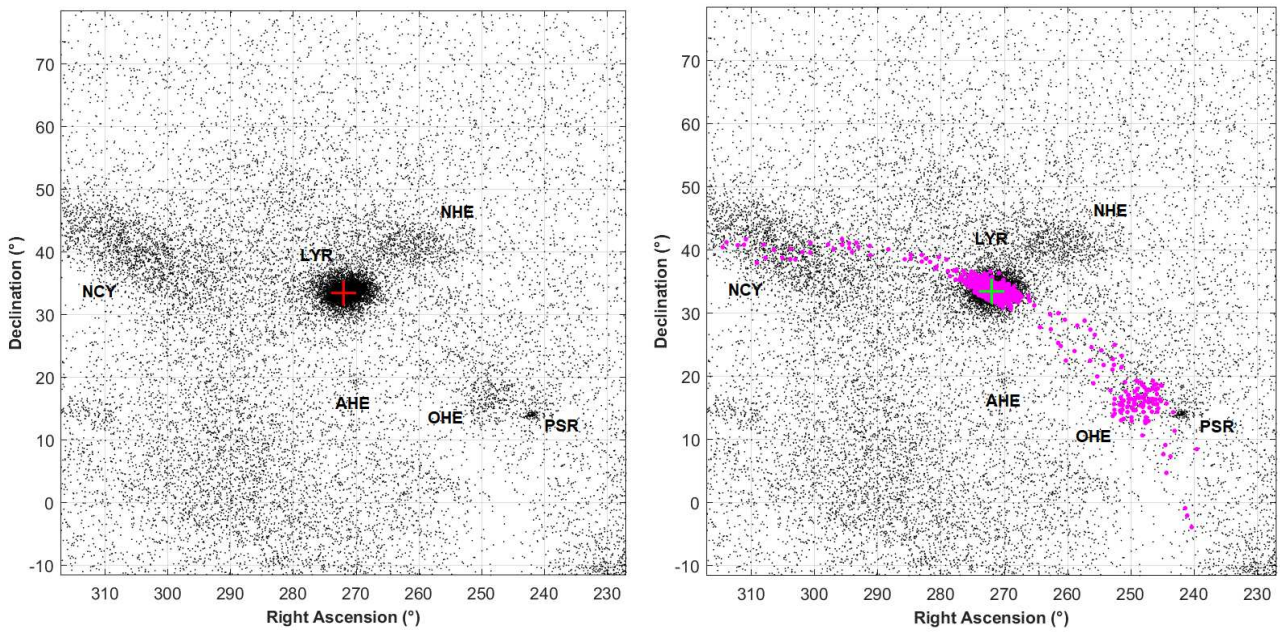


*Figure 1* – Left: The LYR field from solar longitude 22° − 33°. Six areas of activity are labeled. Right: $D_R$ extracted radiants (overlaid with black in print, magenta electronically) showing the association of OHE with LYR. AHE, NHE, NCY and PSR appear to have no association with LYR or comet Thatcher.

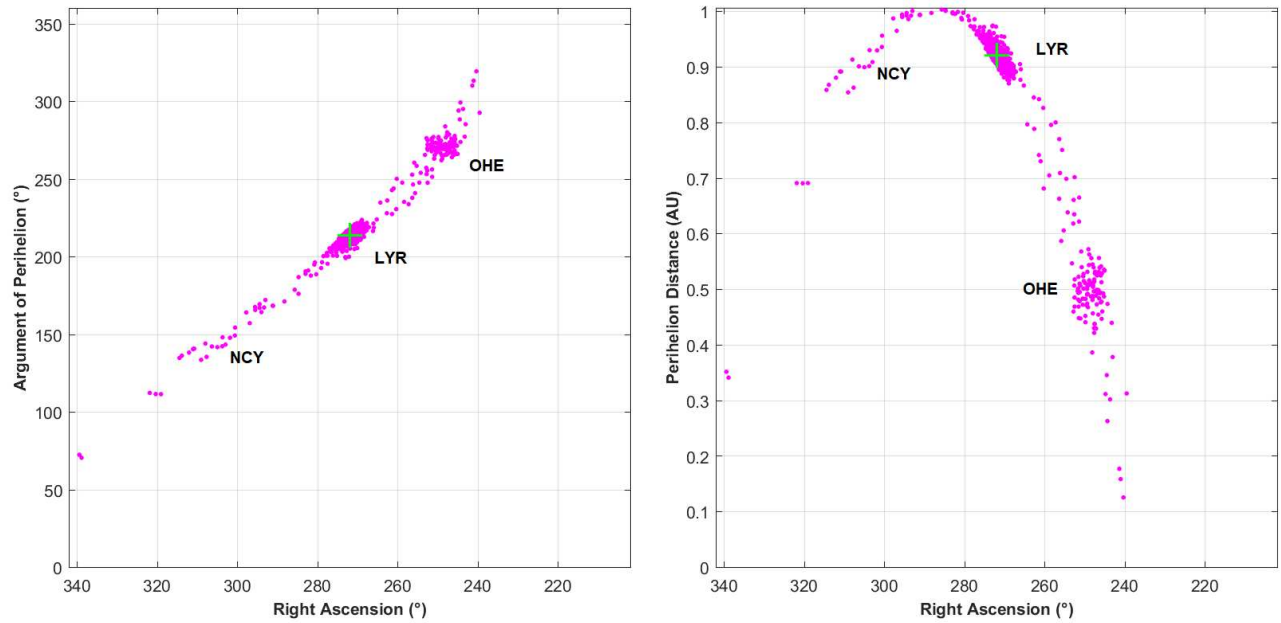


*Figure 2* – The migration of comet Thatcher meteoroids through the secular perturbation $\omega$ cycle is shown by the $D_R$ results for LYR, plotted for $\omega$ (Left) and $q$ (Right). The absence of an accumulated cluster at the NCY location indicates that NCY is not associated with LYR or comet Thatcher. Compare with Figure 4 of Valsecchi et. al (1999).

links LYR with OHE, but does not link LYR with NCY, AHE, NHE, or PSR. The trail of $D_R$ assignments passes over the NCY radiant, but there is no accumulation of assignments over the NCY radiant as for LYR and OHE, so those assigned radiants are background to the NCY.

Indeed, the near-invariants $U$ and $\cos\theta$ for LYR and OHE are in good agreement with each other and with comet Thatcher (Table 1). OHE and LYR mean orbits are nearly in the same plane by inclination and node (±5°), but differ in the argument of perihelion ($\omega$) and the perihelion distance ($q$). The mean shower orbits do not have close encounters with a major planet, so the $\omega$ and $q$ differences are likely due to secular perturbation if both showers are related.

Figure 2 shows how the argument of perihelion and the perihelion distance varies among the meteors extracted in Figure 1. The meteors assigned by $D_R$ trace the secular perturbation cycle of $\omega$. LYR and OHE are at different stages of the cycle. The NCY location is labeled to show there is no accumulation of radiants there.

Figure 3, Left, shows all of the radiants assigned by $D_R$ in Figures 1 and 2 occupying the same location on the $U$-$\cos\theta$ plane, also indicating a common parent

*Table 1* – Mean and median elements for the LYR, OHE, KSE†, and NUH samples with the estimated Standard Error. $N$ was found using $D_N$ at thresholds that recovered a sample subset of the radiants in the cluster, except for KSE†. The orbit of comet C/1861 G1 (Thatcher) is listed on the bottom row.

| Shower | N | $\alpha_g$ [°] | $\delta_g$ [°] | $V_g$ [km/s] | $q$ [AU] | $i$ [°] | $\omega$ [°] | $\Omega$ [°] | $\Pi$ [°] | $1/a$ [AU$^{-1}$] | $U$ [°] | $\cos\theta$ |
|---|---|---|---|---|---|---|---|---|---|---|---|---|
| LYR* | 6422 | 272.19 | 33.23 | 46.41 | 0.9183 | 79.34 | 214.83 | 32.23 | 247.06 | 0.077 | 1.5667 | −0.481 |
| | | ±0.02 | ±0.01 | ±0.01 | ±0.0006 | ±0.02 | ±0.03 | ±0.01 | ±0.03 | ±0.001 | ±0.000 | ±0.000 |
| OHE** | 142 | 249.5 | 16.4 | 46.9 | 0.508 | 75.0 | 269.9 | 28.7 | 298.2 | 0.029 | 1.580 | −0.470 |
| | | ±0.2 | ±0.1 | ±0.1 | ±0.003 | ±0.1 | ±0.4 | ±0.2 | ±0.4 | ±0.005 | ±0.002 | ±0.001 |
| KSE†* | 21 | 247.0 | 18.2 | 46.4 | 0.534 | 74.4 | 266.8 | 24.6 | 291.4 | 0.039 | 1.544 | −0.469 |
| NUH** | 40 | 270.5 | 30.7 | 48.9 | 0.922 | 84.7 | 213.3 | 25.6 | 239.1 | 0.059 | 1.650 | −0.530 |
| | | ±0.2 | ±0.1 | ±0.1 | ±0.002 | ±0.2 | ±0.4 | ±0.1 | ±0.4 | ±0.008 | ±0.004 | ±0.002 |
| C/1861 G1 (Thatcher) | | | | | 0.9207 | 79.77 | 213.45 | 31.87 | 245.32 | 0.018 | 1.582 | −0.481 |

† Shiba (2023)
* arithmetic means
** medians

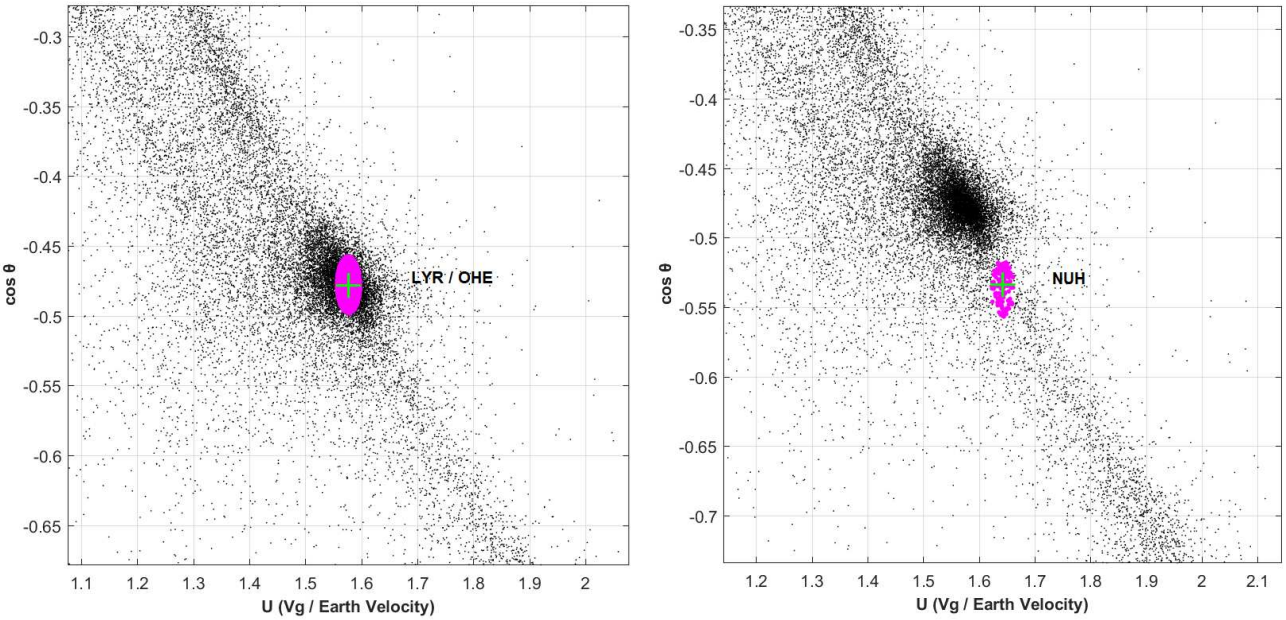


*Figure 3* – Left, All of the radiants assigned by $D_R$ to LYR and OHE, and all of the other radiants of the extended trail shown in Figures 1 and 2, form a compact cluster on the $U$-cos $\theta$ plane (overlaid with grey in print, magenta electronically), indicating a common parent body for all $D_R$ assignments. Right, NUH which forms a nearby but separate cluster on the $U$-cos $\theta$ plane. Compare with Figures 1-3 of Jopek et. al (1999).

body. Compare with Figures 1–3 of Jopek et al. (1999). Jopek et al. pointed out that while $D_R$ results may link meteoroid orbits, it is "...a necessary, but not a sufficient condition to infer that they belong to the same meteoroid stream.", so dynamical modeling would be required to be conclusive.

The mean OHE orbit also descends at about the same distance from Earth's orbit as it ascends, so there could be a related daytime shower 6 months earlier with a radiant at R.A. = 154°, Decl. = −31° and $V_g$ = 46.7 km/s around solar longitude 206° (October 19). No reported shower with similar orbital elements is found around that time in the MDC data. We checked the latest CAMS data and found what may be this twin shower centered at R.A. = 153.6°, Decl. = −22.9° (elongated in Declination), with $V_g$ = 47.7 km/s around solar longitude 199° (October 12). This shower was provisionally named October 44-Hydrids (FHD).

## 4 The nu-Herculids (NUH)

On the day leading to the onset of the Lyrid shower, there is a small cluster of activity just south of the later more diffuse Lyrid shower radiant with the provisional MDC designation M2023-O1, a shower we provisionally call the nu-Herculids (code NUH). NUH is active from solar longitude 23.86° – 28.53° and peaks at 25.8° in that small cluster about 5° south of the beginning of a larger and looser accumulation of LYR radiants that begins at solar longitude 26°.

Figure 3, Right, shows that the NUH cluster is separate from the LYR/OHE cluster on the $U$-cos $\theta$ plane. NUH was active during 2011, 2013–2015, and 2019–2023. $D_N$ at $D_c$ = 0.0567 identified 36 radiants. Five more were found in later CAMS data.

A total of 41 NUH meteors are in a Halley-type orbit, or possibly a long period comet orbit if there is measurement error, with a median $T_J$ = 0.486 and a median orbital period of ∼ 38 years. The median NUH orbit is

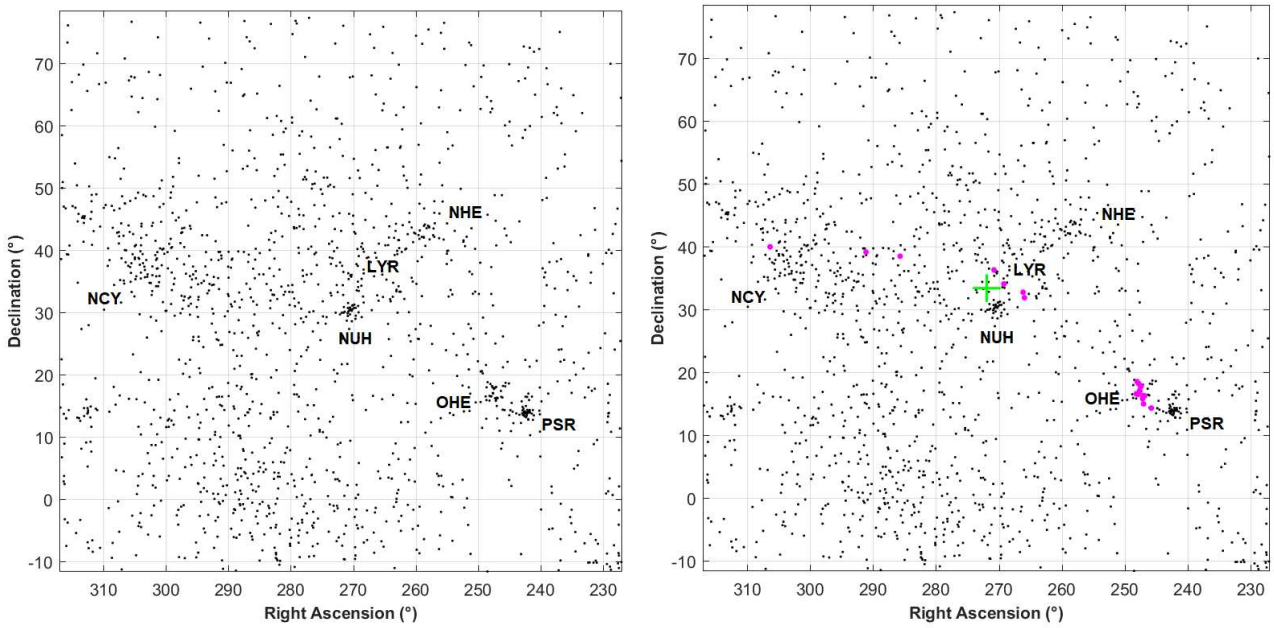


*Figure 4* – Left: Plot of NUH and surrounding field for solar longitude 25.0 − 26.0 degrees. Right: $D_R$ results for LYR just before the onset of LYR activity.

very similar to the mean LYR orbit but has higher inclination (+5.3°) and perhaps a shorter orbital period, with only a bit more than a third of the LYR semi-major axis. Elements $q$, $\omega$, and $e$ are similar, but the near-invariants $1/a$, $U$, and $\cos\theta$ are different mostly due to the difference in $a$. See Table 1 and bottom of Table 2.

The similarity of NUH orbital elements with LYR, but with different near-invariants is difficult to explain. NUH may be meteors from comet Thatcher that had a gravitational interaction that shortened the semi-major axes, which might explain why $D_R$ does not link NUH with LYR.

## 5 Conclusion

The omega-Herculids (OHE) are a previously observed but misclassified shower in the same region but following the kappa-Serpentids (KSE). The nu-Herculids (NUH) are a small cluster of radiants in the same region, but slightly offset from, and seen just prior to the first activity from the April Lyrids (LYR). The MDC has given this shower the provisional designation M2023-O1.

$D_R$ results show that LYR and OHE orbital elements fall along different parts of the $\omega$ cycle undergone by particles from comet Thatcher. On the $U$-$\cos\theta$ plane all of the $D_R$ assignments spread out in the other plots form a compact cluster, also indicating a common parent body. Dynamical modeling is required to be conclusive. The descending OHE stream may have a twin daytime counterpart at the ascending node that appears in later CAMS data and is provisionally named October 44-Hydrids (FHD).

The nu-Herculids (NUH) are a short duration shower that have higher inclination than the LYR, and may not originate directly from comet Thatcher, but are similar to LYR orbits. Only near-invariant quantities distinguish the two. $D_R$ does not link NUH with LYR, so NUH is thought to be new activity that occurs just before the onset of the LYR activity. The NUH radiants and the LYR radiants are separate on the $U$-$\cos\theta$ plane.

## References

Holman D. (2023). "The Meteor Orbit Association Tool v1.0 (MOAT): An Interacitve Graphical User Interface MATLAB Program". *WGN, Journal of the IMO*, **51:5**, 112–117.

Jenniskens P. (2023). *Atlas of Earth's Meteor Showers*. Elsevier, Amsterdam.

Jenniskens P., Baggaley J., Crumpton I., Aldous P., Pokorny P., Janches D., Gural P. S., Samuels D., Albers J., Howell A., Johannink C., Breukers M., Odeh M., Moskovitz N., Collison J., and Ganju S. (2018). "A survey of southern hemisphere meteor showers". *Planetary and Space Science*, **154**, 21–29.

Jenniskens P., Gural P. S., Dynneson L., Grigsby B. J., Newman K. E., Borden M., Koop M., and Holman D. (2011). "CAMS: Cameras for Allsky Meteor Surveillance to establish minor meteor showers". *Icarus*, **216:1**, 40–61.

Jenniskens P. and Haberman B. (2013). ""Thatcher's Ghost": Confirmation of the $\nu$ Cygnids (NCY, IAU #409)". *WGN, Journal of the International Meteor Organization*, **41:3**, 75–76.

Jopek T. J., Valsecchi G. B., and Froeschle C. (1999). "Meteoroid stream identification: a new approach - II. Application to 865 photographic meteor orbits". *Monthly Notices of the Royal Astronomical Society*, **304:4**, 751–758.

*Table 2* – The 41 NUH meteors and median values, with LYR mean values from the sample. $\phi$ is the angle between the $y$-$z$ plane and the plane containing $U$ and the $y$-axis (Öpik, 1976).

| Source: | Year | $\lambda_\odot$ | $q$ | $e$ | $i$ | $\omega$ | $\Omega$ | $a$ | $U$ | $\cos\theta$ | $\theta$ | $\phi$ |
|---|---|---|---|---|---|---|---|---|---|---|---|---|
| CAMS | 2015 | 23.86 | 0.9346 | 0.9679 | 85.44 | 210.50 | 23.85 | 29.12 | 1.67 | −0.54 | 122.4 | 195.7 |
| CAMS | 2015 | 25.75 | 0.9247 | 1.0257 | 86.14 | 212.32 | 25.74 | −.− | 1.70 | −0.54 | 122.4 | 197.0 |
| CAMS | 2021 | 25.42 | 0.9167 | 0.8772 | 84.26 | 215.39 | 25.42 | 7.47 | 1.63 | −0.54 | 122.4 | 197.2 |
| CAMS | 2021 | 25.07 | 0.9132 | 0.9232 | 84.89 | 215.61 | 25.07 | 11.89 | 1.65 | −0.53 | 122.3 | 198.1 |
| CAMS | 2023 | 25.84 | 0.9248 | 0.9133 | 85.54 | 213.29 | 25.84 | 10.67 | 1.66 | −0.54 | 122.9 | 196.6 |
| CAMS | 2023 | 25.84 | 0.9168 | 0.9268 | 86.26 | 214.86 | 25.84 | 12.53 | 1.67 | −0.55 | 123.3 | 197.4 |
| CAMS | 2019 | 25.57 | 0.9190 | 0.9789 | 86.49 | 213.90 | 25.55 | 43.61 | 1.69 | −0.54 | 123.0 | 197.4 |
| SonotaCo | 2011 | 25.15 | 0.9200 | 0.9682 | 84.56 | 213.86 | 25.15 | 28.95 | 1.66 | −0.53 | 121.9 | 197.3 |
| SonotaCo | 2011 | 25.22 | 0.9220 | 0.9078 | 84.73 | 213.95 | 25.22 | 10.00 | 1.64 | −0.54 | 122.5 | 196.8 |
| SonotaCo | 2011 | 25.28 | 0.9250 | 0.9456 | 84.86 | 212.91 | 25.28 | 17.00 | 1.66 | −0.53 | 122.2 | 196.7 |
| SonotaCo | 2014 | 24.39 | 0.9210 | 1.0164 | 84.85 | 213.17 | 24.39 | −.− | 1.68 | −0.52 | 121.7 | 197.4 |
| SonotaCo | 2019 | 25.22 | 0.9330 | 0.9645 | 84.26 | 210.91 | 25.22 | 26.32 | 1.65 | −0.52 | 121.7 | 195.9 |
| EDMOND | 2013 | 25.06 | 0.9221 | 0.8282 | 83.23 | 214.78 | 25.06 | 5.37 | 1.60 | −0.53 | 122.2 | 196.5 |
| EDMOND | 2013 | 25.06 | 0.9173 | 0.8506 | 83.18 | 215.56 | 25.06 | 6.14 | 1.60 | −0.53 | 122.0 | 197.1 |
| EDMOND | 2013 | 27.04 | 0.9327 | 0.9138 | 87.37 | 211.62 | 27.04 | 10.82 | 1.68 | −0.56 | 124.1 | 195.7 |
| EDMOND | 2014 | 25.81 | 0.9287 | 0.9117 | 86.65 | 212.45 | 25.82 | 10.51 | 1.67 | −0.55 | 123.6 | 196.1 |
| EDMOND | 2014 | 25.81 | 0.9299 | 0.9677 | 86.77 | 211.67 | 25.82 | 28.82 | 1.69 | −0.55 | 123.3 | 196.2 |
| GMN | 2020 | 25.22 | 0.9276 | 0.9147 | 84.70 | 212.65 | 25.22 | 10.88 | 1.64 | −0.54 | 122.4 | 196.3 |
| GMN | 2020 | 25.23 | 0.8975 | 0.9004 | 84.84 | 218.97 | 25.23 | 9.01 | 1.64 | −0.54 | 122.7 | 199.2 |
| GMN | 2020 | 26.64 | 0.9253 | 0.9585 | 86.06 | 212.81 | 26.64 | 22.31 | 1.68 | −0.54 | 122.9 | 196.7 |
| GMN | 2021 | 25.00 | 0.9157 | 0.9788 | 82.70 | 214.56 | 25.00 | 43.22 | 1.64 | −0.51 | 120.6 | 197.8 |
| GMN | 2021 | 25.07 | 0.9259 | 0.9504 | 84.10 | 212.68 | 25.07 | 18.66 | 1.65 | −0.53 | 121.7 | 196.6 |
| GMN | 2021 | 25.33 | 0.9240 | 0.9298 | 83.83 | 213.30 | 25.33 | 13.16 | 1.64 | −0.53 | 121.7 | 196.8 |
| GMN | 2021 | 25.34 | 0.9234 | 0.9655 | 83.85 | 213.09 | 25.34 | 26.76 | 1.65 | −0.52 | 121.4 | 197.0 |
| GMN | 2021 | 25.96 | 0.9336 | 1.0366 | 86.05 | 210.33 | 25.96 | −.− | 1.70 | −0.53 | 122.3 | 196.1 |
| GMN | 2021 | 25.97 | 0.9440 | 1.0238 | 83.44 | 208.02 | 25.97 | −.− | 1.66 | −0.51 | 120.7 | 194.9 |
| GMN | 2021 | 26.28 | 0.9114 | 0.9045 | 85.52 | 216.24 | 26.28 | 9.54 | 1.65 | −0.55 | 123.0 | 197.9 |
| GMN | 2021 | 26.31 | 0.9197 | 0.9502 | 83.86 | 214.06 | 26.31 | 18.45 | 1.64 | −0.52 | 121.6 | 197.3 |
| GMN | 2021 | 26.40 | 0.9370 | 0.9465 | 82.03 | 210.29 | 26.40 | 17.50 | 1.61 | −0.51 | 120.4 | 195.5 |
| GMN | 2022 | 25.79 | 0.9175 | 0.8706 | 84.99 | 215.31 | 25.79 | 7.09 | 1.63 | −0.54 | 122.9 | 197.1 |
| GMN | 2022 | 26.65 | 0.9268 | 0.9286 | 86.09 | 212.74 | 26.64 | 12.98 | 1.67 | −0.55 | 123.1 | 196.4 |
| GMN | 2023 | 24.69 | 0.9321 | 0.9133 | 82.75 | 211.60 | 24.69 | 10.75 | 1.62 | −0.52 | 121.1 | 195.8 |
| GMN | 2023 | 24.70 | 0.9190 | 0.9126 | 84.04 | 214.48 | 24.70 | 10.51 | 1.63 | −0.53 | 122.0 | 197.2 |
| GMN | 2023 | 24.79 | 0.9193 | 0.9788 | 84.62 | 213.79 | 24.79 | 43.32 | 1.66 | −0.53 | 121.8 | 197.4 |
| GMN | 2023 | 24.88 | 0.9146 | 0.9144 | 86.96 | 215.39 | 24.88 | 10.68 | 1.68 | −0.56 | 123.9 | 197.6 |
| GMN | 2023 | 25.17 | 0.8997 | 0.8062 | 84.64 | 219.75 | 25.17 | 4.64 | 1.61 | −0.55 | 123.4 | 198.4 |
| GMN | 2023 | 25.69 | 0.9230 | 0.9664 | 85.82 | 213.18 | 25.69 | 27.44 | 1.68 | −0.54 | 122.7 | 197.0 |
| GMN | 2023 | 25.80 | 0.9113 | 0.8853 | 82.41 | 216.44 | 25.80 | 7.94 | 1.60 | −0.52 | 121.2 | 197.9 |
| GMN | 2023 | 25.81 | 0.9191 | 0.9688 | 84.85 | 213.98 | 25.81 | 29.42 | 1.66 | −0.53 | 122.1 | 197.4 |
| GMN | 2023 | 26.69 | 0.9420 | 0.9364 | 82.61 | 209.20 | 26.69 | 14.82 | 1.62 | −0.51 | 120.8 | 194.9 |
| GMN | 2023 | 28.37 | 0.9105 | 0.9553 | 83.59 | 216.00 | 28.38 | 20.35 | 1.64 | −0.52 | 121.4 | 198.3 |
| NUH Medians: | | 25.57 | 0.9220 | 0.9456 | 84.73 | 213.30 | 25.55 | 12.98 | 1.65 | −0.53 | 122.3 | 197.0 |
| LYR Means: | | 32.23 | 0.9183 | 0.9298 | 79.34 | 214.83 | 32.23 | 32.03 | 1.57 | −0.48 | 118.8 | 197.6 |


Kornoš L., Koukal J., Piffl R., and Tóth J. (2014a). "EDMOND Meteor Database". In Gyssens M., Roggemans P., and Zoladek P., editors, *Proceedings of the International Meteor Conference, Poznan, Poland, 22-25 August 2013*. pages 23–25.

Kornoš L., Matlovič P., Rudawska R., Tóth J., Hajduková, M. J., Koukal J., and Piffl R. (2014b). "Confirmation and characterization of IAU temporary meteor showers in EDMOND database". In Jopek T. J., Rietmeijer F. J. M., Watanabe J., and Williams I. P., editors, *Meteoroids 2013 Conference, A.M. University, Poznań, Poland, Aug. 26-30, 2013*. pages 225–233.

McCrosky R. E. and Posen A. (1959). "New photographic meteor showers". *The Astronomical Journal*, **64**, 25–27.

Öpik E. J. (1976). *Interplanetary Encounters*. Elsevier, Amsterdam.

Shiba Y. (2023). "Halley Type and Long Period Meteor Shower Luminous Altitude Characteristics". *WGN, Journal of the IMO*, **51:4**, 93–108.

SonotaCo (2009). "A meteor shower catalog based on video observations in 2007-2008". *WGN, Journal of the International Meteor Organization*, **37:2**, 55–62.

SonotaCo (2016). "Observation error propagation on video meteor orbit determination". *WGN, Journal of the International Meteor Organization*, **44:2**, 42–45.

SonotaCo (2017). "Exhaustive error computation on 3 or more simultaneous meteor observations". *WGN, Journal of the International Meteor Organization*, **45:5**, 95–97.

SonotaCo, Masuzawa T., Sekiguchi T., Miyoshi T., Fujiwara Y., Maeda K., and Uehara S. (2021). "SNMv3: A Meteor Data Set for Meteor Shower Analysis". *WGN, Journal of the International Meteor Organization*, **49:3**, 64–70.

Valsecchi G. B., Jopek T. J., and Froeschlé C. (1999). "Meteoroid stream identification: a new approach - I. Theory". *Mon. Not. R. Astron. Soc.*, **304:4**, 743–750.

Vida D., Gural P. S., Brown P. G., Campbell-Brown M., and Wiegert P. (2020). "Estimating trajectories of meteors: an observational Monte Carlo approach - I. Theory". *Monthly Notices of the Royal Astronomical Society*, **491:2**, 2688–2705.

Vida D., Šegon D., Gural P. S., Brown P. G., McIntyre M. J. M., Dijkema T. J., Pavletić L., Kukić P., Mazur M. J., Eschman P., Roggemans P., Merlak A., and Zubović D. (2021). "The Global Meteor Network - Methodology and first results". *Monthly Notices of the Royal Astronomical Society*, **506:4**, 5046–5074.

*Handling Editor:* Javor Kac

# Estimating Fireball Trajectories Using Seismic and Acoustic Data

*Denis Vida* [1,2]

Of about 73000 well-documented meteorites, only about 50 are instrumentally observed and have a known orbit. Knowing the orbit of a meteorite provides a direct sample of its originating region of the Solar System. Orbits are most often estimated from data obtained by dedicated optical systems with limited area and temporal coverage. In this work, a simple method of fireball trajectory inversion using seismic data is described in detail. Fireball trajectories are modelled as near-cylindrical sources of ballistic waves, the trajectories are inverted from times of arrival of ballistic waves to seismic stations. The method is verified and validated by reproducing previously known seismic and optical trajectories of several fireballs.

Received 2023 October 6

## 1 Introduction

Fireball trajectories are usually determined from optical records – analog or digital images or video. Positions of a fireball are measured at every point in time of its duration, which enables estimating its velocity as well as the radiant, i.e. its point origin in the sky (Ceplecha, 1987; Borovička, 1990; Vida et al., 2020). Specialized fireball networks have been deployed around the world which consist of sensitive high-resolution cameras with wide-angle lenses, e.g. the European Fireball Network (Oberst et al., 1998), Australian Desert Fireball Network (Bland et al., 2012), Prairie Network (McCrosky et al., 1978), Southern Ontario Meteor Network (Brown et al., 2010), and others. Running such networks requires specialized equipment and highly qualified personnel which limits them to regional coverage. On the other hand, trajectories can also be estimated from casual video recordings such as security cameras or hand-held video cameras (Vida et al., 2021), one of the most well-known examples of such an application is on the 2013 Chelyabinsk fireball (Borovička et al., 2013). The downside of optical methods is that they generally only collect data during the day, and are dependent on favourable weather conditions.

Metre-scaled asteroids impact the Earth every $\sim$ 10 days (Brown et al., 2002), which produce fireballs which are only occasionally witnessed by humans and more rarely recorded on video. These larger objects are usually observed by US government sensors and published on the NASA Center for Near Earth Object Studies (CNEOS) website[a], whoever there are concerns about the reported accuracy of this data set (Devillepoix et al., 2019) as recently highlighted by dubious claims of listed objects of nominal interstellar origin (Brown & Borovička, 2023).

Anglin and Haddon (1987) have been the first to report unambiguous observations of seismic waves produced by a fireball-induced ballistic shock recorded by a network of seismographs. Le Pichon et al. (2002) reconstructed a trajectory of a December 2000 fireball in Tahiti using an algorithm for measuring earthquake depths, while Ishihara et al. (2003, 2004) developed a fireball trajectory inversion technique which assumes cylindrical propagation of ballistic waves successfully applied it to reconstruct the trajectory of the 1998 Miyako fireball over Japan. Brown et al. (2003) applied the method to the 2000 Moravka fireball and found the estimated trajectory comparable to the optically estimated trajectory by Borovička et al. (2003). Pujol et al. (2005) laid out the detailed theoretical background behind this trajectory inversion technique and performed a detailed sensitivity analysis. They successfully reconstructed the trajectory of a November 2003 fireball over Arkansas, but concluded that the velocity of the fireball cannot be unambiguously determined with the technique in question. Kalenda et al. (2014) made an overview of the topic and have successfully applied the method to several meteorite-dropping fireballs for which optical records have already existed, confirming the validity of the method, although not giving any concrete values nor comparisons with optical trajectories. Nevertheless, they propose methods for correcting the wave propagation for the varying speed of sound and wind drift. Recently, McFadden et al. (2021) developed a novel method for trajectory inversion using a full atmosphere model and numerical modelling. Their work describes a method that was based on the work presented herein but in a more advanced form using atmospheric propagation instead of assuming a fixed speed of sound and no wind.

In this report, we follow the method of Pujol et al. (2005), which is described in detail in section 2, and apply it to several cases of seismically observed fireballs (section 3). This work was first written as an unpublished report in 2017 and has been subsequently adapted for publication in WGN.

## 2 Trajectory model

When a solid body moves through the air at a speed higher than the speed of sound, the spherical pressure waves in front of the body are combined in a single shock wave. This shock wave propagates from the front of the body in a conic pattern known as the Mach cone. The ratio between the speed of the body and the speed

[1]Department of Physics and Astronomy, University of Western Ontario, London, Ontario, N6A 3K7, Canada. Email: dvida@uwo.ca

[2]Western Institute for Earth and Space Exploration, University of Western Ontario, London, Ontario, N6A 5B7, Canada.

IMO bibcode WGN-515-vida-seismic
NASA-ADS bibcode 2023JIMO...51..132V

[a]CNEOS fireballs: https://cneos.jpl.nasa.gov/fireballs/, accessed October 6, 2023

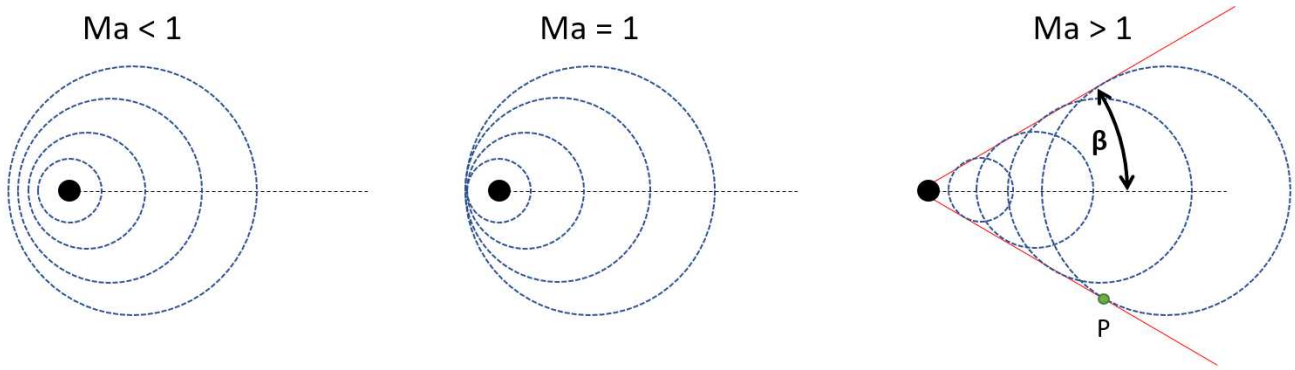


*Figure 1* – Comparison of shock wave propagation depending on the speed of the object.

of sound is known as the Mach number. Figure 1 shows three cases of sound wave propagation: a) when the body travels at subsonic speed, b) when the body travels at the speed of sound, c) when the body travels faster than the speed of sound and the edges of pressure waves form a Mach cone.

Assuming a linear trajectory of the body, the angle between the trajectory and the edges of the waves can be determined using the following equation:

$$\sin\beta = \frac{c}{v} \tag{1}$$

where $c$ is the speed of sound, and $v$ is the speed of the body. The rightmost inset in Figure 1 shows how the angle $\beta$ relates to the trajectory and released waves. Pujol et al. (2005) shows that there is exactly one spherical wave emitted from the trajectory at time $t$ that reaches an observer positioned at the point P, meaning that the waves emitted on different parts of the trajectory will never arrive at the same time. After the arrival of the initial wave, others will arrive with lower amplitude as they are released further on on the trajectory. For the case of fireballs, where $v \gg c$, the Mach angle $\beta$ is very small, around 1°, which means that fireballs can be approximated as cylindrical sources of waves. Nevertheless, in this work, the speed of the fireball and its Mach angle are given full consideration.

As shock waves from a fireball are released, they propagate through the atmosphere and reach the ground. If a seismic station happens to be within the range of these waves, up to a maximum distance of about 150 km, the ballistic wave interacts with the instrument. If several stations have recorded the arrival of the wave, it is possible to model the fireball trajectory and the release of ballistic waves and match them to observations. Thus, by applying this inverse technique, the trajectory of a fireball can be recovered from times of ballistic wave arrivals at seismic stations. Figure 2 shows the fireball trajectory model as developed by Ishihara et al. (2003) and described in detail by Pujol et al. (2005). The fireball trajectory is defined by 6 parameters: $x_0, y_0, t_0, v, \phi, \vartheta$, which are described below.

For simplicity, geographic coordinates (latitude, longitude, elevation) of all seismic stations that have received the shock wave signal are converted to a Cartesian coordinate system (which will be referred to as the local coordinate system) where the positive direction of the X axis points towards the south, the positive direction of the Y axis towards the east, and the positive direction of the Z axis points up. Details of this coordinate transform are given in Appendix A. The origin of the coordinate system is a point on Earth's surface, most often it is the location of one of the seismic stations. The trajectory of the fireball is defined by a direction vector $\vec{u}$:

$$\vec{u} = [\cos\phi\sin\vartheta, \sin\phi\sin\vartheta, -\cos\vartheta] \tag{2}$$

where $\phi$ is the azimuth (+E of due S) and $\vartheta$ is the zenith angle of the trajectory. The trajectory intersects the $Z = 0$ plane (which is tangent to the surface of the Earth at reference geographical coordinates) at point $(x_0, y_0, 0)$. $t_0$ is then time at which a fireball moving at speed $v$ reaches the point $(x_0, y_0, 0)$. The earliest observed time of arrival was taken to be the reference time, thus $t_0$ should always be within a few minutes from that reference time.

From the given parameters of the fireball and the location of the seismic station $(x_s, y_s, z_s)$, the time $t_a$ (time of arrival) when the shock wave released from the fireball reaches the station can be calculated as:

$$\vec{b} = [x_s - x_0, y_s - y_0, z_s] \tag{3}$$

$$d_t = \left|\vec{b}\cdot\vec{u}\right| \tag{4}$$

$$d_p = \sqrt{\left|\vec{b}\right|^2 - d_t^2} \tag{5}$$

$$t_a = t_0 - \frac{d_t}{v} + \frac{d_p\cos\beta}{c} \tag{6}$$

where $\vec{b}$ is the vector pointing from $(x_0, y_0, 0)$ to the station, $d_t$ is the distance between the point $(x_0, y_0, 0)$ and the closest point on the trajectory to the given station, and $d_p$ is the distance between the station and that closest point. $\beta$ is the Mach angle which can be calculated using equation 1, given the speed of the fireball $v$ and the speed of sound $c$. The deceleration of the fireball is disregarded. The term $\frac{d_t}{v}$ is the time that it takes the fireball to reach the point $(x_0, y_0, 0)$ at time $t_0$ from the moment it produced the ballistic wave. $d_p\cos\beta$ is the distance between the station and the position on

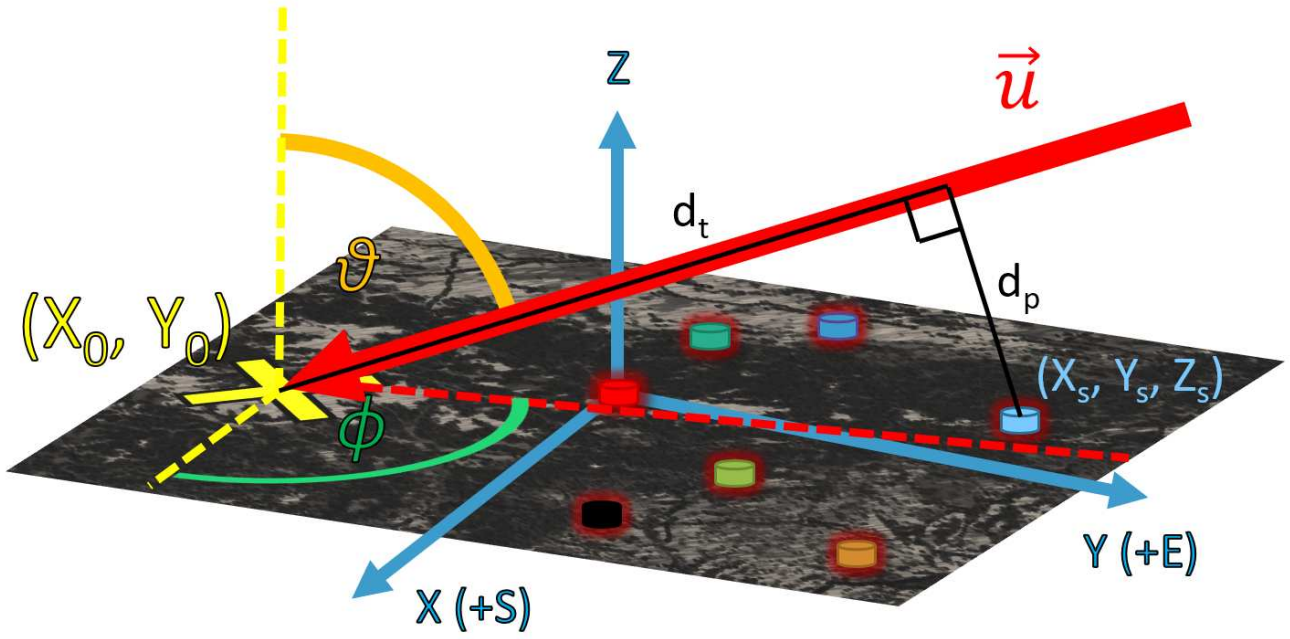


*Figure 2* – Fireball trajectory model in the local coordinate system. Colored disks represent seismic stations, the red arrow is the trajectory of the fireball.

the trajectory from where the ballistic wave is released, with the Mach cone taken into account.

In this work the speed of sound is taken to be a constant $c = 320\,\mathrm{m\,s^{-1}}$, following Pujol et al. (2005). They have demonstrated that the solution is not sensitive to the changes in the speed of sound, which might be ±6% from the nominal value (Kalenda et al., 2014). A possible improvement, implemented by Brown et al. (2003), is to calculate the average speed of sound between the point of wave release and the receiving station. A rough approximation for the varying speed of sound with temperature is given by Kalenda et al. (2014):

$$c(T) = 20.0468\sqrt{T} \tag{7}$$

where the speed of sound is given in $\mathrm{m\,s^{-1}}$, while $T$ is the temperature of the atmosphere in K. Given an atmospheric model or direct measurements obtained from sounding balloons, the average speed of sound can be easily calculated for every release of ballistic waves.

## 2.1 Fitting the trajectory model to observations

Pujol et al. (2005) have approached the problem of fitting the trajectory model to observations numerically, they linearised the trajectory equations and solved them iteratively as a set of partial differential equations. A similar approach is used here, the difference being that the following cost function is minimized directly:

$$L = \sum_{i=1}^{N_{stations}} 2\left(\sqrt{1 + (t_{ac_i} - t_{ao_i})^2} - 1\right) \tag{8}$$

where $t_{ac_i}$ is the calculated and $t_{ao_i}$ the observed time of arrival at station $i$. The given cost function is the smooth approximation of absolute value loss, meaning that differences in the observed and calculated times of arrival that are less than 1 are smoothed out, while larger ones are added in with an approximate absolute value loss. Due to the observed times of arrival being somewhat uncertain, the more frequently used sum of squared differences produced unstable solutions. This is to be expected as the wind drift was not taken into account, which might be significant (Kalenda et al., 2014), and outliers would be weighted by the square of their value, pushing the solution in the wrong direction.

Particle Swarm Optimization (PSO) algorithm (Kennedy & Eberhart, 1995) was used for minimizing the cost function. The bounds for parameters $x_0, y_0$ were set to ±300 km, ±200 s for $t_0$, and the velocity of the fireball was searched within the $11 - 30\,\mathrm{km\,s^{-1}}$ range. The bounds on the azimuth and the zenith angle were set manually for each case, as they are roughly known from eyewitness accounts or optical measurements. Special care was taken to remove the influence of the 0/360° boundary in azimuth by offsetting it with the mean value of the given range. Due to the inherent randomness of the PSO algorithm, where the 2000 particles were uniformly distributed throughout the parameter space, the estimation was run 10 times and the solution with the smallest value of the cost function was chosen as the nominal solution.

## 3 Results

The implementation of the method was verified by using data of the 2003 Arkansas fireball provided by Pujol et al. (2005) and comparing the results of two implementations, which is described in section 3.1. Next, in section 3.2 the method was applied to the 2000 Moravka fireball, the seismic data was provided by Brown et al. (2003) and the fireball trajectory was compared to the

optical trajectory estimated by Borovička et al. (2003). Finally, the method was applied to the 1998 Miyako and 2013 Montreal fireballs (sections 3.3 and 3.4, respectively).

### 3.1 2003 Arkansas fireball

As a way of verifying our implementation of the Pujol et al. (2005) method, seismic data from their paper was used. The fireball in question was observed over north-east Arkansas in November 2003 and the ballistic waves were picked up by 18 seismic stations. The inversion with our implementation was found to be stable, the final solution for the trajectory being $\phi = 272.3°, \vartheta = 40.9°$. Pujol et al. (2005) obtained the values of $\phi = 269.5°, \vartheta = 49.0°$. The azimuth agrees well, but there is a 8.1° difference in the zenith angle. We have found this suspiciously close to $90° - \vartheta$ of our value, and as both solutions were stable, this might mean that the $\vartheta$ value reported in Pujol et al. (2005) is actually the elevation, not the zenith angle. The ground map of the solution is shown in Figure 3. Root mean square (RMS) of our solution was 0.21 s, with the highest residual of 0.48 s, comparable to the 0.27 − 0.30 s RMS obtained by (Pujol et al., 2005), and their highest residual of 0.52 s. The first height of ballistic wave release is estimated to be 78.3 km, while the last one is 47.9 km, both of which are within the physical limits of ballistic wave release.

### 3.2 2000 Moravka fireball

The Moravka meteorite fall was observed in May 2000 in the Czech Republic by various ground and space-based instruments (Brown et al., 2003), including seismographs and infrasound microphones. The trajectory and the velocity of the fireball were accurately reconstructed by Borovička et al. (2003) from optical data, which enables direct comparison to other methods of trajectory estimation. Brown et al. (2003) have applied the seismic trajectory method as well, but they have found that the velocity of the fireball significantly differs from the one determined optically (only 8.3 km s$^{-1}$, compared to optically estimated 18 km s$^{-1}$), which is consistent with conclusions of (Pujol et al., 2005) about the coupling of the fireball velocity and time $t_0$.

The arrival of the ballistic wave of the fireball was picked up by 8 stations, starting about 90 s after the fireball. We have obtained values of $\phi = 183.8°$ and $\vartheta = 71.2°$, which compare favourably to optically determined values of $\phi = 184.5°$ and $\vartheta = 69.6°$ (Borovička et al., 2003). Furthermore, this also compares well to

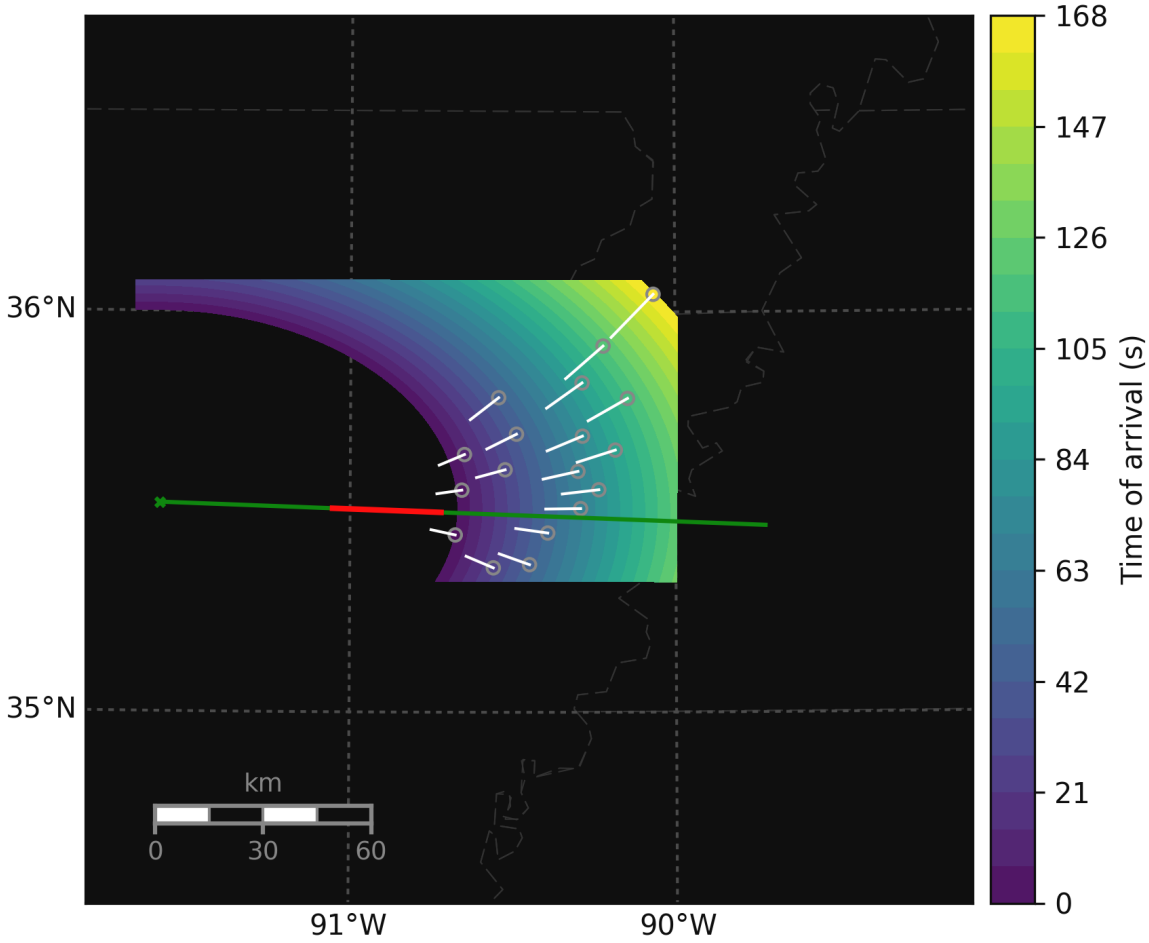


*Figure 3* – Ground map of the Arkansas fireball. The green line is the trajectory of the fireball, the green X is the $(x_0, y_0, 0)$ point, while the red line segment represents the part of the trajectory from which the stations picked up the ballistic waves. Gray circles are the positions of the stations, while white lines are ground projections of vectors pointing to the position on the trajectory from where the received ballistic wave was released from.

values estimated by Brown et al. (2003), which were $\phi = 188.0°$ and $\vartheta = 70.2°$. Nevertheless, during the parameter estimations we have found many local minima for the solution of the zenith angle, solutions often converging to a 45° zenith angle. The RMS of the final solution was 1.42 s, with the highest residual of 2.1 s. The top and bottom heights of wave release were 25.6 km and 21.7 km.

### 3.3 1998 Miyako fireball

Ishihara et al. (2003) were the first to develop the trajectory inversion method used in this report. They have applied it to the March 1998 Miyako fireball which was observed both seismically and optically. Reconstructing the trajectory from 21 seismic stations they have achieved a good match to the optical trajectory: $\phi = 287°$ and $\vartheta = 71.5°$, compared to optically estimated $\phi = 296°$ and $\vartheta = 71.7°$. Their approach to parameter estimation was a grid brute-force search on all of the parameters with a fixed step size, choosing the solution with the lowest sum of squared residuals – the RMS of their best solution is 1.1 s. Surprisingly, we have failed to obtain any stable solution using the data provided by the authors. All convergences had a very high RMS ($> 100$ s), even when constraining the parameter space to within a few degrees of the values cited above. This conclusion is striking, as the method was verified and validated on other cases with robust convergences. We suggest independently verifying our results and the results presented in Ishihara et al. (2003). Moreover, the authors also claim good convergence of the velocity which no other authors were able to achieve on any other events. A possible explanation might be a typographic error in the data given in the Ishihara et al. (2003) paper which prevented us from reproducing their numbers.

### 3.4 2013 Montreal fireball

On 26 November 2013 sightings of a bright flash in the sky were reported in Montreal, several minutes later followed by a sound of an explosion. The region was heavily overcast, thus no photographic evidence of the event exists. Edwards et al. (2014) investigated the event with the hypothesis that it was an energetic fireball. They have found waveform signatures in USArray seismic data which resembled ballistic shocks and have attempted to apply the method of Pujol et al. (2005) to invert the trajectory of the fireball. They concluded that 5 stations were not enough for a robust solution, and the lack of east-west coverage was especially detrimental to the quality of the trajectory. Nevertheless, the authors have roughly estimated that the fireball had an almost straight north-south trajectory, with a shallow elevation of $< 30°$. After applying our implementation of the method on the same data, we have surprisingly found a convergence to a solution with the RMS of

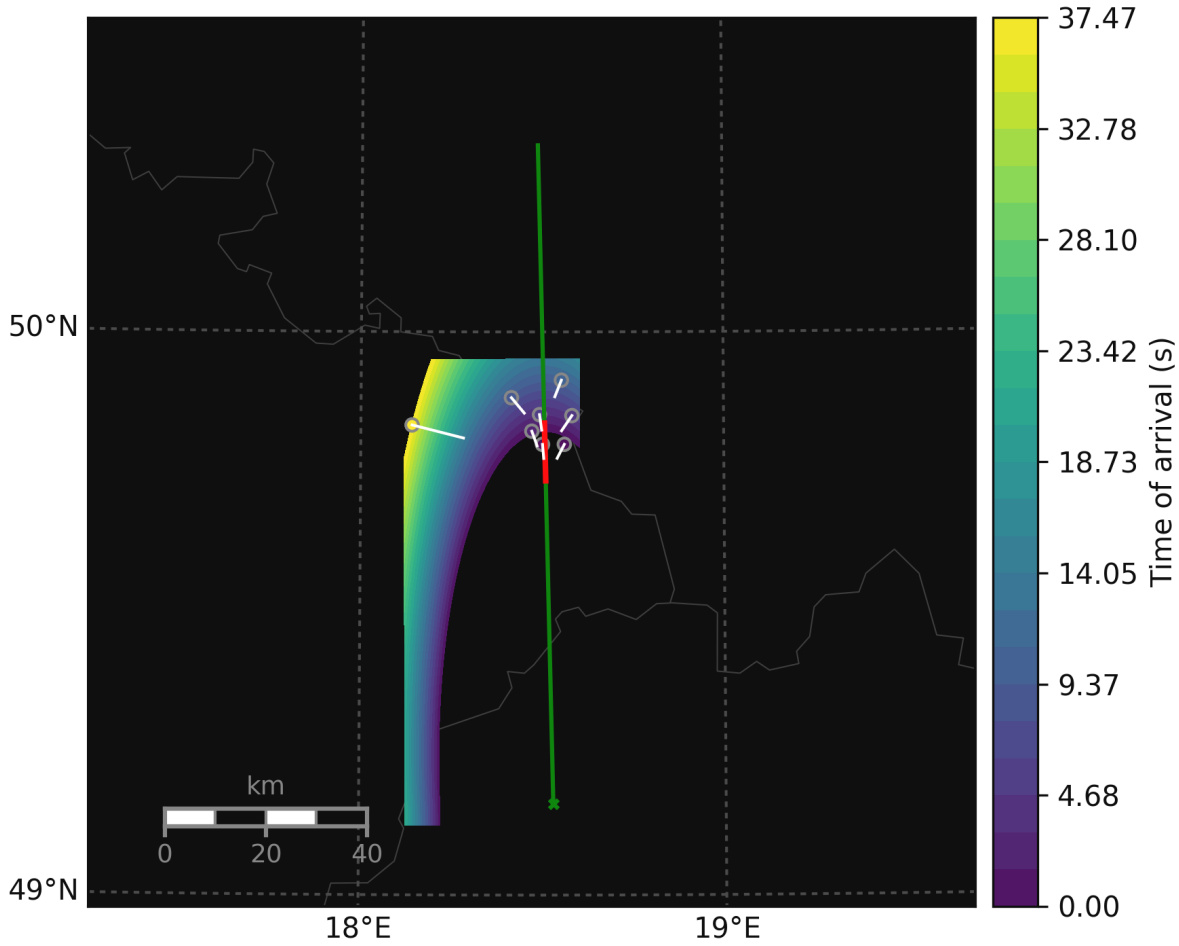


*Figure 4* – Ground map of the Moravka meteorite-dropping fireball.

0.0 s. Upon further investigation, it was discovered that the solution is not unique and there are multiple convergences with a seemingly good fit, but we believe that the low number of seismic stations might be the cause. Many of the solutions were also not physical, with the points of wave release only 1 or 2 kilometres above the ground, while fireballs usually do not penetrate deeper than 15 km before decelerating to subsonic speeds. We conclude that great care must be taken when applying this trajectory model to non-ideal data, especially when the number of receiving stations is low.

## 4 Conclusion

We have successfully implemented, verified and validated a seismic fireball trajectory inversion method assuming a fixed speed of sound and no wind. Good matching with the results of Pujol et al. (2005) for the 2003 Arkansas fireball was achieved, as well as for the 2000 Moravka fireball for both optical (Borovička et al., 2003) and seismic (Brown et al., 2003) solutions. We have failed to reproduce the results of Ishihara et al. (2003) for the 1998 Miyako fireball, possibly due to data issues. Finally, we concluded that great care needs to be taken when applying the model to fireballs with a low number and non-ideal distribution of receiving seismic stations, as there were many good convergences to non-physical trajectories of the 2013 Montreal fireball.

Future work includes applying the model to a meteorite-dropping fireball for which the trajectory is not known. The most common use of this method is predicted to be for estimating trajectories of fireballs that happened during the day when many night-time monitoring systems are offline, as well as events that happen during unfavourable weather conditions. In those cases, the direction of the trajectory can be determined seismically, but the velocity has to be independently estimated using either casual video recordings or other single-station optical data.

## References


Anglin F. M. and Haddon R. A. W. (1987). "Meteoroid sonic shock-wave-generated seismic signals observed at a seismic array". *Nature*, **328:6131**, 607–609.

Bland P. A., Spurnỳ P., Bevan A. W. R., Howard K. T., Towner M. C., Benedix G. K., Greenwood R. C., Shrbenỳ L., Franchi I. A., Deacon G., et al. (2012). "The Australian Desert Fireball Network: a new era for planetary science". *Australian Journal of Earth Sciences*, **59:2**, 177–187.

Borovička J. (1990). "The comparison of two methods of determining meteor trajectories from photographs". *Bulletin of the Astronomical Institutes of Czechoslovakia*, **41**, 391–396.

Borovička J., Spurnỳ P., Kalenda P., and Tagliaferri E. (2003). "The Morávka meteorite fall: 1. Description of the events and determination of the fireball trajectory and orbit from video records". *Meteoritics & Planetary Science*, **38:7**, 975–987.

Borovička J., Spurnỳ P., and Shrbenỳ L. (2013). "Trajectory and orbit of the Chelyabinsk superbolide". *Electronic Telegram, Cambridge, MA: Central Bureau Electronic Telegrams.–Int. Astron.–Union*, **3423**.

Brown P., Spalding R. E., ReVelle D. O., Tagliaferri E., and Worden S. P. (2002). "The flux of small near-Earth objects colliding with the Earth". *Nature*, **420:6913**, 294–296.

Brown P., Weryk R. J., Kohut S., Edwards W. N., and Krzeminski Z. (2010). "Development of an all-sky video meteor network in Southern Ontario, Canada The ASGARD System". *WGN, Journal of the International Meteor Organization*, **38**, 25–30.

Brown P. G. and Borovička J. (2023). "On the proposed interstellar origin of the USG 20140108 fireball". *The Astrophysical Journal*, **953:2**, 167.

Brown P. G., Kalenda P., Revelle D. O., and Borovička J. (2003). "The Morávka meteorite fall: 2. Interpretation of infrasonic and seismic data". *Meteoritics & Planetary Science*, **38:7**, 989–1003.

Ceplecha Z. (1987). "Geometric, dynamic, orbital and photometric data on meteoroids from photographic fireball networks". *Bulletin of the Astronomical Institutes of Czechoslovakia*, **38**, 222–234.

Devillepoix H. A. R., Bland P. A., Sansom E. K., Towner M. C., Cupák M., Howie R. M., Hartig B. A. D., Jansen-Sturgeon T., and Cox M. A. (2019). "Observation of metre-scale impactors by the Desert Fireball Network". *Monthly Notices of the Royal Astronomical Society*, **483:4**, 5166–5178.

Edwards W. N., de Groot-Hedlin C. D., and Hedlin M. A. H. (2014). "Forensic investigation of a probable meteor sighting using USArray acoustic data". *Seismological Research Letters*, **85:5**, 1012–1018.

Ishihara Y., Furumoto M., Sakai S., and Tsukada S. (2004). "The 2003 Kanto large bolide's trajectory determined from shockwaves recorded by a seismic network and images taken by a video camera". *Geophysical research letters*, **31:14**.

Ishihara Y., Tsukada S., Sakai S., Hiramatsu Y., and Furumoto M. (2003). "The 1998 Miyako fireball's trajectory determined from shock wave records of a dense seismic array". *Earth, Planets and Space*, **55:5**, e9–e12.

Kalenda P., Borovička J., and Spurný P. (2014). "The localization of fireball trajectories with the help of seismic networks". *Studia Geophysica et Geodaetica*, **58:1**, 84–99.

Kennedy J. and Eberhart R. C. (1995). "Particle swarm optimization". In *Proceedings of the IEEE International Conference on Neural Networks*. pages 1942–1948.

Le Pichon A., Guérin J. M., Blanc E., and Reymond D. (2002). "Trail in the atmosphere of the 29 December 2000 meteor as recorded in Tahiti: Characteristics and trajectory reconstitution". *Journal of Geophysical Research: Atmospheres*, **107:D23**.

McCrosky R. E., Shao C.-Y., and Posen A. (1978). "Prairie Network fireballs. I-general information and orbits". *Meteoritika*, **37**, 44–59.

McFadden L., Brown P., Vida D., and Spurnỳ P. (2021). "Fireball characteristics derivable from acoustic data". *Journal of Atmospheric and Solar-Terrestrial Physics*, **216**, 105587.

Oberst J., Molau S., Heinlein D., Gritzner C., Schindler M., Spurny P., Ceplecha Z., Rendtel J., and Betlem H. (1998). "The "European Fireball Network": current status and future prospects". *Meteoritics & Planetary Science*, **33:1**, 49–56.

Pujol J., Rydelek P., and Bohlen T. (2005). "Determination of the trajectory of a fireball using seismic network data". *Bulletin of the Seismological Society of America*, **95:4**, 1495–1509.

Vida D., Gural P. S., Brown P. G., Campbell-Brown M., and Wiegert P. (2020). "Estimating trajectories of meteors: an observational Monte Carlo approach–I. Theory". *Monthly Notices of the Royal Astronomical Society*, **491:2**, 2688–2705.

Vida D., Šegon D., Šegon M., Atanackov J., Ambrožič B., McFadden L., Ferrière L., Kac J., Kladnik G., Živčić M., et al. (2021). "Novo Mesto meteorite fall-trajectory, orbit, and fragmentation analysis from optical observations". In *European Planetary Science Congress*. pages EPSC2021–139.

*Handling Editor:* Javor Kac
This paper has been typeset from a LaTeX file prepared by the author.

# A Conversion of geographical to and from the local coordinate system

Let $\varphi_s$ be the latitude of a seismic station, $\lambda_s$ the longitude, and $h_s$ its elevation in metres. Let ($\varphi_0$, $\lambda_0$, $h_0$) be the reference coordinates, which are the coordinates of the origin of the local coordinate system (these can be the coordinates of one of the stations). The positive direction of the X axis points towards the south, Y towards the east and Z points up (see figure 2).

The distance from the centre of the Earth to the position given by geographical coordinates in the WGS84 system is calculated as follows:

$$N = \frac{r_e}{\sqrt{1 - e_e^2 \sin^2 \varphi}} \tag{A.1}$$

where $r_e$ is the equatorial radius of the Earth as defined by the WGS84 system, $r_e = 6378137.0\,\mathrm{m}$, and $e_e$ is the equatorial ellipticity of an oblate Earth:

$$e_e = \sqrt{1 - \frac{r_e^2}{r_p^2}} \tag{A.2}$$

where $r_p$ is the polar radius of the Earth, $r_p = 6356752.314245\,\mathrm{m}$. The polar ellipticity is:

$$e_p = \sqrt{1 - \frac{r_e^2 - r_p^2}{r_p^2}} \tag{A.3}$$

## A.1 Geographical to local coordinate conversion

First, all geographical coordinates are converted to earth-centred earth-fixed (ECEF) coordinates:

$$\begin{aligned} x_{ECEF} &= (N + h) \cos\varphi \cos\lambda \\ y_{ECEF} &= (N + h) \cos\varphi \sin\lambda \\ z_{ECEF} &= \Big((1 - e_e^2)N + h\Big) \sin\varphi \end{aligned} \tag{A.4}$$

after which all station coordinates are converted to be relative to ECEF coordinates of the reference position, ($x_{0ECEF}, y_{0ECEF}, z_{0ECEF}$):

$$\begin{bmatrix} x'_{ECEF} \\ y'_{ECEF} \\ z'_{ECEF} \end{bmatrix} = \begin{bmatrix} x_{ECEF} \\ y_{ECEF} \\ z_{ECEF} \end{bmatrix} - \begin{bmatrix} x_{0ECEF} \\ y_{0ECEF} \\ z_{0ECEF} \end{bmatrix} \tag{A.5}$$

Relative ECEF coordinates are converted to the east, north, and up (ENU) coordinates:

$$\begin{bmatrix} x_{ENU} \\ y_{ENU} \\ z_{ENU} \end{bmatrix} = \begin{bmatrix} -\sin\lambda_0 & \cos\lambda_0 & 0 \\ -\sin\varphi_0 \cos\lambda_0 & -\sin\varphi_0 \sin\lambda_0 & cos\varphi_0 \\ \cos\varphi_0 \cos\lambda_0 & \cos\varphi_0 \sin\lambda_0 & \sin\varphi_0 \end{bmatrix} \begin{bmatrix} x'_{ECEF} \\ y'_{ECEF} \\ z'_{ECEF} \end{bmatrix} \tag{A.6}$$

Finally, ENU coordinates are rotated by 90° around the Z axis to obtain coordinates in the desired local coordinate system:

$$\begin{bmatrix} x_L \\ y_L \\ z_L \end{bmatrix} = \begin{bmatrix} \cos\frac{\pi}{2} & \sin\frac{\pi}{2} & 0 \\ -\sin\frac{\pi}{2} & \cos\frac{\pi}{2} & 0 \\ 0 & 0 & 1 \end{bmatrix} \begin{bmatrix} x_{ENU} \\ y_{ENU} \\ z_{ENU} \end{bmatrix} \tag{A.7}$$

## A.2 Local to geographical coordinate conversion

To convert the local coordinates to geographical coordinates, an inverse transformation to the one described in section A.1 is applied. First, the local coordinates are rotated by −90° around the Z axis to obtain ENU coordinates:

$$\begin{bmatrix} x_{ENU} \\ y_{ENU} \\ z_{ENU} \end{bmatrix} = \begin{bmatrix} \cos -\frac{\pi}{2} & \sin -\frac{\pi}{2} & 0 \\ -\sin -\frac{\pi}{2} & \cos -\frac{\pi}{2} & 0 \\ 0 & 0 & 1 \end{bmatrix} \begin{bmatrix} x_L \\ y_L \\ z_L \end{bmatrix} \tag{A.8}$$

Next, ENU coordinates are converted to ECEF coordinates:

$$\begin{bmatrix} x_{ECEF} \\ y_{ECEF} \\ z_{ECEF} \end{bmatrix} = \begin{bmatrix} -\sin\lambda_0 & -\sin\varphi_0\cos\lambda_0 & \cos\varphi_0\cos\lambda_0 \\ \cos\lambda_0 & -\sin\varphi_0\sin\lambda_0 & \cos\varphi_0\sin\lambda_0 \\ 0 & \cos\varphi_0 & \sin\varphi_0 \end{bmatrix} \begin{bmatrix} x_{ENU} \\ y_{ENU} \\ z_{ENU} \end{bmatrix} + \begin{bmatrix} x_{0ECEF} \\ y_{0ECEF} \\ z_{0ECEF} \end{bmatrix} \tag{A.9}$$

Finally, ECEF coordinates are converted to geographical coordinates. The longitude $\varphi$ is calculated simply as:

$$\varphi = \arctan\left(\frac{y_{ECEF}}{x_{ECEF}}\right) \tag{A.10}$$

The latitude $\lambda$ is then:

$$\begin{aligned} p &= \sqrt{x_{ECEF}^2 + y_{ECEF}^2} \\ \theta &= \arctan\left(\frac{z_{ECEF} r_e}{p r_p}\right) \\ \lambda &= \arctan\left(\frac{z_{ECEF} + e_p^2 \sin^3\theta}{p - e_e^2 r_e \cos^3\theta}\right) \end{aligned} \tag{A.11}$$

Finally, the elevation above sea level is calculated as:

$$h = \frac{p}{\cos\lambda} - N \tag{A.12}$$

although care must be taken when $\lambda \approx \pm 90°$, as equation A.12 is not defined for exact poles, and values of cosine near 90° may be numerically imprecise. In that case, height can be calculated as:

$$h = |z| - r_p \tag{A.13}$$

## B Points of wave emission

The position from where the wave received by a station was emitted on the trajectory can be calculated to determine if the obtained solution produced physical heights of wave release, which should be between $\sim 20$ km and $\sim 80$ km.

Let $\vec{r}$ be the vector pointing from $(X_0, Y_0, 0)$ to the point of wave emission:

$$\vec{r} = -\vec{u}\left(d_t + d_p \tan\beta\right) \tag{B.1}$$

then the position of the wave emission is simply:

$$\vec{w} = [x_0, y_0, 0] + \vec{r} \tag{B.2}$$

# Preliminary results

## Observation of a short activity burst of the September Lyncids or Beta Aurigids?

*Jürgen Rendtel*[1]

A roughly 20-minute activity burst was observed on 2023 September 25 centred $00^h28^m$ UT ($\lambda_\odot = 181\,^\circ\!.374$). It included three moderately bright meteors (−2 to 0 mag) which were also recorded by cameras of the AllSky7 network. They fit with a radiant east of $\beta$ Aurigae, probably with the September Lyncids (081 SLY), perhaps with the $\beta$-Aurigids (210 BAU). For the interval $00^h20^m$ – $00^h36^m$ UT this yields a ZHR of about 20.

Received 2023 October 13

### A Introduction

In September and October we find several meteor showers with highly inclined orbits (Rendtel & Molau, 2010) with radiants in the region including Perseus, Auriga and Lynx. Essentially, this series starts with the activity of the September $\varepsilon$-Perseids (208 SPE). Outbursts of this shower have been observed in 2008 (Rendtel & Molau, 2010) and 2013 (Rendtel et al., 2014). Further weak showers with radiants in the same region include the $\delta$-Aurigids (224 DAU) as well as three radiants in the constellation Lynx. The activity of all these sources seems to vary from one year to the next and they are probably are not caused by one common source.

At the end of September, the list of showers in the IAU MDC data base[a] includes the September Lyncids (081 SLY), the September-October-Lyncids (424 SOL), the $\beta$-Aurigids (210 BAU), the $\psi$-Aurigids (425 PSA) and finally the 34 Lyncids (901 TLC) further to the east. Rendtel & Molau (2010) speculated that these showers with $130^\circ < i < 150^\circ$ originate from a group of comets on high inclination orbits. Activity from these radiants was – at least in some periods around end September into early October – easily recogniseable in visual observations.

### B Observations in 2023

Like in previous years, I noted a small number of meteors radiating from east of Auriga in a few nights from 2023 September 15 onwards. They fitted a radiant which may be identified with the September Lyncids (081 SLY), or the $\beta$-Aurigids (210 BAU). The numbers yielded a ZHR of about 2–3 with a better fit of the 081 SLY.

In the night September 24-25 I was surprised when five of these meteors occurred within 16 minutes. It started at $00^h20^m$ UT when two bright meteors (−2 and −1 mag) occurred almost synchronously in the western sky. The last one of this series (0 mag) was seen at $00^h36^m$ UT. All three bright meteors were found on images taken by the nearby cameras of the AllSky7 network (Figure 1). The camera station 238 in Ketzür is just about 20 km from my observing location near Töplitz (52°26′51″N; 12°55′15″E).

*Figure 1* – Two bright meteors with a radiant east of Auriga occurred almost synchronously on 2023 September 25, at $00^h20^m$ UT as seen on this stacked image of the AMS238 camera in Ketzür, Germany. ©AllSky7 Fireball Network allsky7.net, AMS238 Sirko Molau.

Considering an interval of 20 minutes covering the bright meteors as well as two other possible shower meteors yields a ZHR of about 20. Correction factors have almost no effect here since the limiting magnitude was +6.4 (the Sky Quality Meter gave 20.7) and the radiant elevation was above 50°.

### C Other observations

The CAMS data at `https://meteorshowers.seti.org/?lat=1.800&long=97.200&date=2023-09-25` show (Figure 2) several meteors annotated as 210 BAU ($\beta$-Aurigids). On September 30, the IAU MDC database stated that "there are too few orbits to consider the 210 BAU a significant detection". Now, on October 12, the shower is back in the working list, with no remark on the number of orbits any more. However, there is some activity from radiants in the area in the sky over the above mentioned period. It is not from a clear dominating radiant, but rather from variable positions.

Concerning the recognition of the described activity, I can say that the long term experience, combined with years of plotting meteor trajectories helps to get alert if something happens. Similar experiences have been reported by other visual observers. Observations

[1]International Meteor Organization, Eschenweg 16, 14476 Potsdam, Germany. Email: `jrendtel@web.de`

IMO bibcode WGN-515-rendtel-sly
NASA-ADS bibcode 2023JIMO...51..141R

[a]`https://www.ta3.sk/IAUC22DB/MDC2007/Roje/roje_lista.php?corobic_roje=0&sort_roje=0`

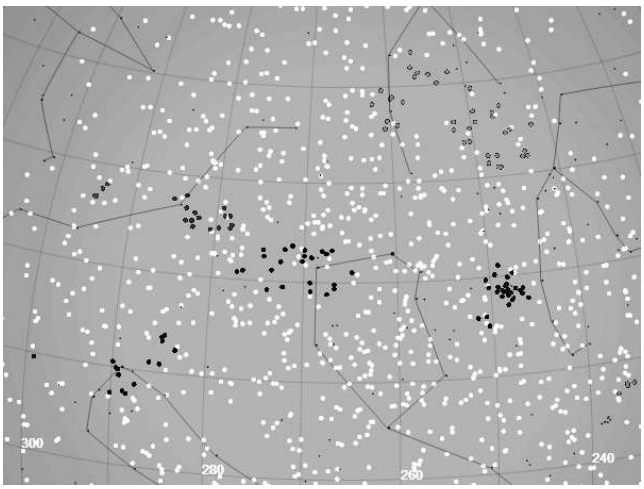


*Figure 2* – Part of the radiant plot from `https://meteorshowers.seti.org/?lat=1.800&long=97.200&date=2023-09-25` (accessed last on 2023 October 10). The dark spots represent radiants listed in the working list. The velocities are colour-coded in the web graph. In our graph, the darkest points refer to meteors with the highest velocities. Radiants of fast meteors east of Auriga (associated with 210 BAU) and further east into Lynx (labelled 424 SOL) reach the Earth at about 65 km/s. The white dots represent radiants of sporadic meteors (not associated with a known shower).

of some previous events probably gave some training. Among these there were the 20 minute outburst of the $\alpha$-Monocerotids in 1995 (Rendtel et al., 1996), the weak but significant October Camelopardalids 2018 (Rendtel & Molau, 2018) but also the almost insignificant $\kappa$-Cepheids (751 KCE) on 2015 September 21 (Rendtel, 2015). Some further detections of weak activity include the $\gamma$-Ursae Minorids (404 GUM) in January and the November $\varsigma$-Ursae Majorids (488 NSU) in end November 2022. This shows that such weak events may occur not a once in your lifetime but more often.

## D Conclusion

Meteors from far northern radiants in September – October can be observed regularly. Usually, the ZHR is of the order of 2–3. Occasionally, there may be intervals with higher rates as observed on 2023 September 25 around $00^{\mathrm{h}}20^{\mathrm{m}}$ – $00^{\mathrm{h}}40^{\mathrm{m}}$ UT when the ZHR reached 20 or slightly more. The activity is probably associated with the September Lyncids (081 SLY) or the $\beta$-Aurigids (210 BAU).

So it is worth to perform regular visual observations and to take notes about meteor trajectories in order to associate meteors with radiants defined e.g. by video meteor observations. There are certainly minor sources active with radiants in Auriga-Lynx between mid-September until mid-October, although it currently is difficult to decide which of these may be included in the working list of meteor showers.

## Acknowledgements

Thanks to André Knöfel for immediately checking the recordings of the AllSky7 cameras and providing me with the shown image of the observed meteor pair.

## References

Rendtel J. (2015). "Minor kappa-Cepheid (751 KCE) activity on 2015 September 21". *WGN, Journal of the International Meteor Organization*, **43:6**, 177–178.

Rendtel J., Brown P., and Molau S. (1996). "The 1995 outburst and possible origin of the alpha-Monocerotid meteoroid stream". *Monthly Notices of the Royal Astronomical Society*, **279:3**, L31–L36.

Rendtel J., Lyytinen E., Molau S., and Barentsen G. (2014). "Peculiar activity of the September epsilon-Perseids on 2013 September 9". *WGN, Journal of the International Meteor Organization*, **42:2**, 40–47.

Rendtel J. and Molau S. (2010). "Meteor activity from the Perseus-Auriga region in September and October". *WGN, Journal of the International Meteor Organization*, **38:5**, 161–166.

Rendtel J. and Molau S. (2018). "October Camelopardalid outburst 2018 October 6". *WGN, Journal of the International Meteor Organization*, **46:5**, 173–175.

*Handling Editor:* Javor Kac
This paper has been typeset from a LaTeX file prepared by the author.

# The International Meteor Organization

www.imo.net

Follow us on Facebook InternationalMeteorOrganization

Follow us on Twitter @IMOMeteors

## Council

*President:* Cis Verbeeck,
Bogaertsheide 5, 2560 Kessel, Belgium.
e-mail: cis.verbeeck@gmail.com

*Vice-President:* Juraj Tóth,
Fac. Math., Phys. & Inf., Comenius Univ.,
Mlynska dolina, 84248 Bratislava, Slovakia.
e-mail: toth@fmph.uniba.sk

*Secretary-General:* Robert Lunsford,
14884 Quail Valley Way, El Cajon,
CA 92021-2227, USA. tel. +1 619 755 7791
e-mail: lunro.imo.usa@cox.net

*Treasurer:* Marc Gyssens, Heerbaan 74,
B-2530 Boechout, Belgium.
e-mail: marc.gyssens@uhasselt.be
BIC: GEBABEBB
IBAN: BE30 0014 7327 5911
Bank transfer costs are always at your expense.

*Other Council members:*
Karl Antier, 16, rue de la République,
F-04100 Manosque, France.
e-mail: karl.antier@gmx.fr
Javor Kac (see details under WGN)
Detlef Koschny, Zeestraat 46,
NL-2211 XH Noordwijkerhout, Netherlands.
e-mail: detlef.koschny@tum.de
Sirko Molau, Abenstalstraße 13b, D-84072
Seysdorf, Germany. e-mail: sirko@molau.de
Francisco Ocaña Gonzalez, C/ Arquitectura, 7.
28005 Madrid, Spain.
e-mail: francisco.ocana.gonzalez@gmail.com
Vincent Perlerin, 16, rue Georges Bernanos,
51100 Reims, France.
e-mail: vperlerin@gmail.com
Jürgen Rendtel, Eschenweg 16, D-14476
Marquardt, Germany. e-mail: jrendtel@aip.de

## Commission Directors

*Visual Commission:* Jürgen Rendtel
Generic e-mail address: visual@imo.net
Electronic visual report form:
http://www.imo.net/visual/report/electronic
*Video Commission:* Sirko Molau (video@imo.net)
*Photographic Commission:* Bill Ward
(bill_meteor@yahoo.com)
Generic e-mail address: photo@imo.net
*Radio Commission:* Chris Steyaert
(radio@imo.net)
*Fireball Commission:* Robert Lunsford
Online fireball reports:
http://fireballs.imo.net

## Webmaster

Karl Antier, e-mail: webmaster@imo.net

# WGN

*Editor-in-chief:* Javor Kac
Na Ajdov hrib 24, SI-2310 Slovenska Bistrica,
Slovenia. e-mail: wgn@imo.net;
include METEOR in the e-mail subject line

*Editorial board:* Ž. Andreić, D.J. Asher,
F. Bettonvil, M. Gyssens, C. Hergenrother,
T. Heywood, J. Rendtel, C. Verbeeck,
S. de Vet, D. Vida.

# IMO Sales

| *Available from the Treasurer or the Electronic Shop on the IMO Website* | € | $ |
|---|---|---|
| **IMO membership, including subscription to WGN Vol. 51 (2023)** | | |
| Surface mail | 26 | 30 |
| Air Mail (outside Europe only) | 49 | 56 |
| Electronic subscription only | 21 | 24 |
| **Proceedings of the International Meteor Conference** on paper | | |
| 1990, 1991, 1995, 1996, 1999, 2000, 2002, 2003, per year | 9 | 12 |
| 2007, 2010, 2011, per year | 15 | 20 |
| 2012, 2013, 2015, 2017 per year | 25 | 32 |
| **Proceedings of the Meteor Orbit Determination Workshop 2006** | 15 | 20 |
| **Radio Meteor School Proceedings 2005** | 15 | 20 |
| **Handbook for Meteor Observers** | 23 | 29 |
| **Meteor Shower Workbook** | 12 | 16 |
| **Electronic media** | | |
| Meteor Beliefs Project ZIP archive | 6 | 8 |

# 2022 December 24 fireball from Colorado

This colorful fireball with a terminal burst was captured on 2022 December 24 at $08^{h}24^{m}$ UT from Cortez, Colorado, USA. Notice how the winds in the upper atmosphere caused a slight bend in the persistent train. Image courtesy: Rich Davis.